UNIVERSITY OF BIRMINGHAM
University of Birmingham Research at Birmingham

Bod1l is required to suppress deleterious resection of stressed replication forks

Higgs, Martin; Reynolds, John; Winczura, Alicja; Blackford, AN; Borel, Valerie; Miller, Edward; Zlatanou, Anastasia; Nieminuszczy, Jadwiga; Ryan, Ellis; Davies, Nicholas; Stankovic, Tatjana; Boulton, Simon; Niedzwiedz, Wojciech; Stewart, Grant

DOI:
10.1016/j.molcel.2015.06.007

License:
None: All rights reserved

Document Version
Early version, also known as pre-print

Citation for published version (Harvard):
Higgs, M, Reynolds, J, Winczura, A, Blackford, AN, Borel, V, Miller, E, Zlatanou, A, Nieminuszczy, J, Ryan, E, Davies, N, Stankovic, T, Boulton, S, Niedzwiedz, W & Stewart, G 2015, 'Bod1l is required to suppress deleterious resection of stressed replication forks', *Molecular Cell*, vol. 59, no. 3, pp. 462-477. https://doi.org/10.1016/j.molcel.2015.06.007

Link to publication on Research at Birmingham portal

General rights
Unless a licence is specified above, all rights (including copyright and moral rights) in this document are retained by the authors and/or the copyright holders. The express permission of the copyright holder must be obtained for any use of this material other than for purposes permitted by law.

•Users may freely distribute the URL that is used to identify this publication.
•Users may download and/or print one copy of the publication from the University of Birmingham research portal for the purpose of private study or non-commercial research.
•User may use extracts from the document in line with the concept of 'fair dealing' under the Copyright, Designs and Patents Act 1988 (?)
•Users may not further distribute the material nor use it for the purposes of commercial gain.

Where a licence is displayed above, please note the terms and conditions of the licence govern your use of this document.

When citing, please reference the published version.

Take down policy
While the University of Birmingham exercises care and attention in making items available there are rare occasions when an item has been uploaded in error or has been deemed to be commercially or otherwise sensitive.

If you believe that this is the case for this document, please contact UBIRA@lists.bham.ac.uk providing details and we will remove access to the work immediately and investigate.

Download date: 09. May. 2024

BOD1L IS REQUIRED TO SUPPRESS DELETERIOUS RESECTION OF STRESSED REPLICATION FORKS

Martin R. Higgs[1,4], John J. Reynolds[1,4], Alicja Winczura[2¤], Andrew N. Blackford[2§], Valérie Borel[3], Edward S. Miller[1¤], Anastasia Zlatanou[1], Jadwiga Nieminuszczy[2], Ellis L. Ryan[1], Nicholas J. Davies[1], Tatjana Stankovic[1], Simon J. Boulton[3], Wojciech Niedzwiedz[2], Grant S. Stewart[1*].

[1] School of Cancer Sciences, University of Birmingham, Birmingham, B15 2TT, UK

[2] The Weatherall Institute of Molecular Medicine, University of Oxford, Oxford, OX3 9DS, UK.

[3] London Research Institute, Clare Hall Laboratories, South Mimms, Herts, EN6 3LD, UK.

[4] Co-first author.

[*] Correspondence: g.s.stewart@bham.ac.uk

[§] Current address: Wellcome Trust/Cancer Research UK Gurdon Institute, University of Cambridge, Cambridge, CB2 1QN, UK.

[¤] Current address: Division of Biomedical Cell Biology, The University of Warwick, Coventry, CV4 7AL, UK.

RUNNING TITLE: BOD1L prevents DNA-2 dependent fork resection

CHARACTER COUNT: 59,966

SUMMARY

Recognition and repair of damaged replication forks is essential to maintain genome stability, and is coordinated by the combined action of the Fanconi Anaemia and homologous recombination pathways. These pathways are vital to protect stalled replication forks from uncontrolled nucleolytic activity, which otherwise causes irreparable genomic damage. Here we identify BOD1L as a component of this fork protection pathway, which safeguards genome stability after replication stress. Loss of BOD1L confers exquisite cellular sensitivity to replication stress and uncontrolled resection of damaged replication forks, due to a failure to stabilise Rad51 at these forks. Blocking DNA2-dependent resection, or down regulation of the helicases BLM and Fbh1, suppresses both catastrophic fork processing and the accumulation of chromosomal damage in BOD1L-deficient cells. Thus, our work implicates BOD1L as a critical regulator of genome integrity that restrains nucleolytic degradation of damaged replication forks.

INTRODUCTION

Replication stress is any pathological process that compromises the fidelity of genome duplication (Zeman and Cimprich, 2014). The Fanconi Anaemia (FA)/homologous recombination (HR) pathway plays a central role in combatting replication stress (Gari and Constantinou, 2009). FA is a rare chromosomal instability syndrome characterized by severe developmental abnormalities, tumour predisposition and a hypersensitivity to agents that induce DNA inter-strand cross-links (ICLs), such as mitomycin C (MMC) and cisplatin. To date, mutations in at least 16 different genes (FA complementation groups A-Q) have been identified in patients exhibiting features consistent with FA (reviewed in Walden and Deans, 2014).

Whilst historically the FA/HR pathway has been associated with the HR-dependent repair of ICLs, it plays a broader role in protecting cells from replication stress. Indeed, HR-deficient (and some FA) cell lines are hypersensitive to replication stress-inducing agents that do not induce ICLs (e.g. aphidicolin [APH] and hydroxyurea [HU]) (Howlett *et al.*, 2005). It has been proposed that FA and HR proteins function to: (i) protect stalled/collapsed forks from uncontrolled nucleolytic attack (which may render such forks unrecoverable and/or prone to inappropriate repair) (Schlacher *et al.*, 2011; 2012); and (ii) in some cases may facilitate their restart once repair is complete. Cells defective in these processes exhibit an increase in under-replicated DNA, particularly at common fragile sites (CFS). This can result in the generation of ultra-fine anaphase bridges (UFBs), and can ultimately manifest as chromosome breakage and micronuclei (Naim and Roselli, 2009a). The accumulation of such genetic damage over time eventually triggers cell death, and may contribute to the attrition of highly replicating cells, such as germ and haematopoietic cells (Garaycoechea and Patel, 2014).

Despite extensive research, it is still not completely understood how the cell regulates repair of replication damage via the FA/HR pathway. A wide variety of DNA damage response (DDR) and DNA repair proteins, including components of the FA/HR pathway, are recruited to stalled forks upon replication stress (Sirbu *et al.*, 2013). However, it is unclear how replication forks requiring repair are marked: this might involve RPA coated ssDNA, specific DNA secondary structures or damage-inducible post-translational modifications of the replication machinery and/or

surrounding chromatin. It is also likely that some repair proteins are constitutive components of the replication fork machinery, to allow immediate initiation of the DDR once a lesion is encountered.

We have identified an uncharacterised factor, BOD1L, associated with newly replicated chromatin. Cells lacking BOD1L accumulate catastrophic levels of genome damage following replication stress, particularly after MMC exposure, manifesting as excessive chromosome breakage. Although related to the mitotic regulator BOD1, we demonstrate that BOD1L does not regulate spindle orientation but rather functions to protect stalled/damaged replication forks from uncontrolled DNA2-dependent resection. We further show that BOD1L functions within the FA pathway as part of the fork protection machinery, to stabilize Rad51 on chromatin by suppressing the anti-recombinogenic and pro-resection activities of Fbh1 and BLM. Taken together, our data establish that BOD1L is a critical factor associated with the replication machinery that acts to promote fork stability by counteracting negative regulators of HR.

RESULTS

BOD1L is an uncharacterised factor that maintains genome stability following replication stress

Isolation of proteins on nascent DNA (iPOND) is a robust method for the detection of proteins at sites of newly replicated DNA (Sirbu *et al.,* 2013). However, many proteins are sensitive to the harsh conditions of iPOND. To overcome this issue, we first modified the original iPOND protocol and subsequently utilised this new method coupled with mass spectrometry to identify factors associated with nascent chromatin. As with other iPOND-based proteomic studies (Sirbu *et al.*, 2013), we identified numerous replication machinery components at ongoing forks, including the MCM helicase, PCNA, the RFC complex, RPA and the replicative polymerases, polδ and polα (**Figure S1A**). In addition to these proteins, we also identified Biorientation Defect 1-like (BOD1L); a large, previously uncharacterised protein with N-terminal homology to the mitotic regulator BOD1 (**Figure 1A**) (Porter *et al*, 2007). Consistent with these data, we confirmed the presence of BOD1L in EdU precipitates by Western blotting (**Figure 1B**). To verify that BOD1L associated with replication fork proteins, we performed proximity-ligation assays with antibodies against PCNA and BOD1L. We readily detected nuclear PLA signals in undamaged EdU-positive cells, which were strongly reduced in EdU-negative and BOD1L-depleted cells (**Figures 1C-D**). Moreover, we could co-immunoprecipitate BOD1L, and murine GFP-tagged Bod1L, with Mcm2 and Mcm7 (**Figures 1E and S1B**). Together, these data indicate that BOD1L is localised at/near replication forks.

In addition to its homology to BOD1, the amino acid sequence of BOD1L also contains several *in vivo* ATM/ATR phosphorylation sites (Matsuoka *et al.* (2007)), suggesting that BOD1L might play a role in the DDR. To investigate this, we depleted cells of BOD1L using siRNA and analysed cellular sensitivity to a range of DNA damaging agents. Knockdown of BOD1L exquisitely hypersensitised cells to agents that induce replicative stress, in particular MMC (**Figures 1F and S1C**), and was significantly more severe than loss of FANCA. However, co-depletion of FANCA and BOD1L revealed that these two factors were epistatic for MMC hypersensitivity, suggesting that BOD1L may function within the FA pathway. Treatment of BOD1L-depleted cells with replication stress-inducing agents also induced increased micronuclei formation, indicating a critical role for BOD1L in maintaining genome stability upon replication damage (**Figure 1G**).

Importantly, these observations were recapitulated in several cell lines, and in two independent DT40 BOD1L knockout clones (**Figures S1D-H**), demonstrating that the genome instability observed is specifically due to loss of BOD1L, and is neither cell line nor organism specific.

BOD1L and BOD1 are functionally distinct

BOD1 is a mitotic factor that associates with metaphase chromosomes and is essential for correct orientation of the mitotic spindle (Porter *et al*, 2007; Porter *et al*, 2013). Given the sequence similarity of the N-terminus of BOD1L to BOD1, it was conceivable that the increased micronuclei observed in BOD1L-depleted cells arose from mitotic abnormalities.

To first investigate whether BOD1L was functionally related to BOD1, we performed phenotypic analyses of cells depleted of either BOD1 or BOD1L by siRNA. Whilst loss of BOD1L resulted in elevated DDR signalling, specifically the phosphorylation of H2AX and RPA2, this defect was not observed in BOD1-depleted cells (**Figure 2A**). Furthermore, loss of BOD1 neither increased MMC-induced micronuclei, nor engendered a cellular hypersensitivity to MMC or HU (**Figures 2B-D**). In addition, unlike BOD1 depletion, loss of BOD1L did not cause mitotic or spindle alignment defects (**Figures 2E-F**). Finally, immunostaining analyses of MMC-treated cells revealed that BOD1L depletion increases the proportion of micronuclei that are acentric (CENPA-negative) and that contain DNA double strand breaks (DSBs) (53BP1-positive), suggesting that these micronuclei originated from unrepaired DNA damage (**Figure 3A**). Together, these observations demonstrate that BOD1 and BOD1L perform separate roles in cell cycle regulation and genome maintenance respectively.

BOD1L functions within the Fanconi Anaemia pathway

Micronuclei are observed in the absence of several genome stability factors, although FA-deficient are especially prone to ICL-induced micronucleation (Naim and Rosselli, 2009a). It has been proposed that micronuclei arising in cells undergoing replication stress stem from a failure to complete timely DNA replication. This results in the persistence of under-replicated DNA in cells as they enter mitosis, which can manifest as UFBs, typically marked by PICH and flanked by FANCD2 foci (Chan *et al.,* 2007; Chan *et al.,* 2009). These can lead to chromosome breakage and

packaging of the damaged DNA into 53BP1 bodies visible in the subsequent G1 phase (Lukas *et al.*, 2011).

We next determined the prevalence of late replicating DNA, UFBs and G1-phase 53BP1 bodies in BOD1L deficient cells following MMC exposure. Loss of BOD1L dramatically increased the percentage of mitotic cells positive for either FANCD2/PICH positive UFBs or for EdU foci following MMC exposure (**Figures 3B-D**). Consistent with this, we observed a significant rise in the number of 53BP1 G1 bodies in these cells, which was again more severe than depletion of FANCA alone (**Figures 3E-F**). Collectively, these data suggest that the micronuclei observed in BOD1L-deficient cells are due to a failure to correctly resolve replication stress.

FA cells exhibit chromosomal hypersensitivity to agents that induce ICLs, caused in part by the presence of under-replicated DNA, and exhibit chromatid breakage at specific loci, namely CFS (Barlow *et al.*, 2013; Durkin *et al.,* 2007; Schoder *et al.*, 2010). Strikingly, loss of BOD1L resulted in catastrophic levels of chromosome breakage following MMC exposure, which was markedly more severe than FANCA loss (**Figures 3G and S2A**). In agreement with previous data, co-depletion of FANCA/BOD1L had no additional effect on genome instability. Furthermore, the majority of BOD1L-deficient cells showed evidence of chromosome breakage at the CFS locus FRA16D (**Figure 3H**). Importantly, genome stability in BOD1L-depleted cells was restored by the stable expression of murine Bod1L, which is resistant to siRNA-mediated degradation, in two independent HeLa cell clones (CFlap-mBod1L C1-4 and C5-20) (**Figures S2B-D**). Taken together, these observations clearly demonstrate that BOD1L functions to resolve replication stress, in conjunction with FA pathway components (Naim and Rosselli, 2009b).

Given that BOD1L is epistatic with a core FA pathway component, we evaluated the functional integrity of this pathway in the absence of BOD1L. The DNA damage-induced mono-ubiquitylation of FANCD2 is a central event within the FA pathway, and is often used as a marker of FA pathway integrity (Smogorzewska *et al.*, 2007). Loss of BOD1L had no effect on the focal recruitment of FANCD2 to sites of MMC damage, nor its ability to be mono-ubiquitylated (**Figures S2E-F**), suggesting that BOD1L functions downstream of the FA core and FANCI/D2 complexes within the FA/HR pathway.

BOD1L depletion compromises the fidelity of DNA replication following replication stress

The cellular response to replication stress is primarily coordinated by the ATR kinase, which activates the intra-S phase checkpoint and protects stalled replication forks from collapse. Recent studies on ATR-deficient cells have demonstrated that fork protection is crucial to maintain CFS integrity (Koundrioukoff et al., 2013). Given that BOD1L-depleted cells exhibit CFS instability, this suggests that BOD1L may protect replication forks directly, in a similar fashion to ATR. We therefore hypothesised that loss of BOD1L would negatively impact S-phase regulation and/or replication fork dynamics upon replication stress.

Initially, we sought to determine the effect of depleting BOD1L on cell cycle progression. Compromising BOD1L expression had little effect on cell cycle progression in the absence of DNA damage (**Figure 4A**). However, consistent with a defect in resolving S-phase damage, cells lacking BOD1L rapidly accumulated in G2-phase following MMC exposure, with a concomitant reduction in mitotic index (**Figures 4B and S3A-B**); a phenotype reminiscent of FA cells (Akkari *et al.*, 2001; Heinrich *et al.*, 1998;). Next, to directly analyse the stability of on-going replication forks following HU treatment, we quantified the symmetry of sister replication forks originating from the same origin and travelling in opposite directions. Since sister forks typically display similar replication rates (Conti *et al.*, 2007), marked fork asymmetry indicates that individual forks are more prone to stalling (Rodriguez-Lopez *et al.,* 2002). Supportive of a role for BOD1L in promoting fork stability, we observed a significant increase in replication fork asymmetry in BOD1L depleted cells following HU treatment (**Figure 4C**), suggesting that damaged forks are slower to restart and/or are more susceptible to stalling in its absence.

We also observed a significant increase in new origin firing in response to both HU and MMC in cells lacking BOD1L, which was dependent on Cdk1/2 activity (**Figures 4D-E and S3C-E**). However, this origin firing was not due to defective ATR/Chk1 signalling, since BOD1L-depleted cells were proficient for Chk1 phosphorylation on both S317 and S345 in response to MMC (**Figure 4F**). This phenotype was also not present in cells depleted of BOD1, further strengthening the functional divergence of these proteins (**Figure S3F**).

Despite observing increased new origin firing and replication fork asymmetry in BOD1L depleted cells after replication stress, there was no concomitant reduction in the number of

restarted forks, nor any increase in fork stalling (first label terminations). One possible explanation was that new origins were firing proximal to stalled/collapsed (red only labelled) forks in BOD1L depleted cells, therefore artificially enhancing the quantification of restarted (red and green labelled) replication forks. To investigate this, we used a Cdk1/2 inhibitor to inhibit new origin firing in cells lacking BOD1L, and examined the impact on fork stalling/restart. Accordingly, we found that inhibition of Cdk1/2 activity during HU exposure ablated new origin firing, increased the prevalence of stalled replication forks, and decreased fork restart (**Figure S3G**), suggesting that BOD1L prevents fork stalling upon replication stress.

Together, these data suggest that, upon the induction of replication stress, a lack of BOD1L compromises fork stability and/or restart, which triggers dormant origin firing proximal to the stalled/damaged fork.

BOD1L protects stalled forks from uncontrolled resection

It is thought that uncontrolled origin firing in the absence of ATR leads to excessive ssDNA generation and exhaustion of cellular pools of RPA, which both cause irreversible fork collapse (Toledo *et al.*, 2013). It is conceivable that global depletion of soluble RPA may also underlie the excessive chromosome breakage observed in BOD1L deficient cells, since they also exhibit increased origin firing, fork instability and defective fork restart. To investigate this, we first sought to determine levels of ssDNA present in BOD1L-depleted cells following MMC exposure. Loss of BOD1L resulted in a significant increase in RPA loading onto damaged chromatin compared to control cells (**Figures 5A-B and S4A**). Moreover, ablation of BOD1L expression significantly enhanced the formation of MMC-induced native BrdU foci (**Figures 5C and S4B**), consistent with increased ssDNA generation in these cells. However, in contrast to ATR-deficient cells (Toledo *et al*., 2013), RPA over-expression had no effect on either new origin firing or chromosomal instability in the absence of BOD1L (**Figures S4C-E**). In addition, it is clear that the ATR-Chk1 pathway is functional in BOD1L deficient cells (see **Figure 4F**). Therefore, although cells lacking ATR or BOD1L display phenotypic similarities, it appears that the mechanisms underlying replication fork stalling/collapse differ.

It has been demonstrated that loss of FA pathway components such as BRCA2 and FANCD2 leads to nucleolytic degradation of stalled replication forks, rendering them non-permissive for repair by HR (Schlacher *et al.*, 2011; 2012). This excessive fork resection underlies the increased chromosome breakage exhibited by BRCA2-null cells. The nucleases Mre11 and/or DNA2 appear to perform this uncontrolled resection; inhibition of Mre11 can alleviate fork degradation in BRCA2 deficient cells (Schlacher *et al.*, 2011), and depletion of DNA2 rescues the hypersensitivity of FANCD2 deficient cells to cisplatin (Karanja *et al.*, 2014). To investigate whether similar mechanisms underlie the phenotypes of BOD1L-deficient cells, we examined levels of MMC-induced RPA2 phosphorylation on S4/S8, a well-established marker of DNA resection. Depletion of BOD1L (but not BOD1) resulted in elevated levels of RPA2-S4/8 phosphorylation following MMC treatment (**Figures 5D-F and 2A**), which could be restored to control levels by the expression of CFlap-mBod1L (**Figure S4F**). Hyper-phosphorylation of RPA2 was also observed in BOD1L-deficient cells following exposure to HU, indicating that this defect is not restricted to MMC-induced ICLs (**Figure S4G**). Therefore, these data suggest that BOD1L functions to suppress resection. Consistent with this, we observed an increased localisation of BOD1L to damaged forks undergoing resection (**Figure 5G**).

To confirm that uncontrolled resection in BOD1L depleted cells occurs specifically at replication forks, we used the approach described by Schlacher *et al.* (2011) to monitor degradation of nascent DNA. In line with previous observations, loss of BRCA1 or BRCA2 increased the degradation of newly synthesized DNA at forks (apparent as a decreased IdU:CldU ratio; **Figure 6A and S5A-B**). Interestingly, cells lacking BOD1L exhibited similar degradation of stalled replication forks. Critically, this was epistatic with either BRCA1 or BRCA2 depletion, suggesting that BOD1L and BRCA1/2 function within the same pathway to protect replication forks. In support, BRCA2 and BOD1L co-depletion had no additional effect on cellular hypersensitivity to MMC or RPA2 hyper-phosphorylation compared to loss of the individual genes alone (**Figure S5C-E**). Finally, BOD1L co-immunoprecipitated with the fork protection factors FANCD2 and BRCA2 (**Figure 6B**). Together, this provides strong evidence that BOD1L plays a vital role in preventing unconstrained resection at stalled forks, in concert with FANCD2 and BRCA1/2.

We next sought to ascertain whether the increased resection seen in cells devoid of BOD1L was mediated by Mre11, DNA2 and/or Exo1; three nucleases implicated in fork resection. In line with the study by Karanja *et al.* (2014), co-depletion of DNA2, but not Exo1, completely repressed MMC-induced RPA2 S4/8 hyper-phosphorylation observed in cells lacking BOD1L (**Figures S5F-G**). Furthermore, the over-resection of stalled forks was completely abolished by co-depletion of DNA2 with BOD1L. However, in contrast to previous findings with BRCA1/2 and FANCD2 (Schlacher *et al.*, 2011), inhibition of Mre11 by Mirin was unable to rescue nucleolytic fork degradation in the absence of BOD1L (**Figures 6C and S5H**). Moreover, the combined loss of DNA2 and BOD1L restored the MMC-induced micronuclei and chromosome damage to normal levels (**Figure 6D-E**). This demonstrates that the severe genome instability in cells lacking BOD1L arises from uncontrolled DNA2-dependent resection of damaged forks.

BOD1L stabilises Rad51 at damaged replication forks by suppressing anti-recombinogenic pathways

The strand exchange protein Rad51 is best known as a principal effector of HR, but it also plays a central role in stabilising/promoting the restart of damaged replication forks (Petermann *et al.*, 2010; Costanzo, 2011). Accordingly, the excessive fork degradation observed in BRCA2 or FANCD2 deficient cells is restored by overexpressing an ATPase-dead Rad51 mutant, which stabilises Rad51 nucleofilaments on ssDNA by preventing its ATP-dependent dissociation (Schlacher *et al.*, 2011; 2012). Thus, the loading of Rad51 onto stalled forks prevents uncontrolled nucleolytic activity.

To investigate whether a defect with Rad51 function underlies the excessive fork resection observed in the absence of BOD1L, we exposed BOD1L-depleted cells to MMC, and then monitored the accumulation/retention of Rad51 at sites of damage by immunofluorescence. Notably, MMC-induced Rad51 foci formation was severely compromised in BOD1L-depleted cells (**Figure 6F**). This was observed with 4 different BOD1L siRNA sequences, and was not due to any alteration in Rad51 protein expression (**Figures S5I-J**). Moreover, the defective focal recruitment of Rad51 (**Figure S6A**) upon damage could be restored by the expression of CFlap-mBod1L (**Figures S6B-C**). In keeping, Rad51 also failed to load efficiently onto MMC-damaged chromatin

277 in cells lacking BOD1L (**Figure 6G**). Consistent with this, BOD1L-depleted cells exhibited
278 increased numbers of MMC-induced radial chromosomes, and a concomitant decrease in the
279 frequency of MMC-induced SCEs (**Figures S6D-E**). Strikingly, the formation of IR-induced Rad51
280 foci at DSBs was unaffected in BOD1L-depleted cells (**Figure S6F**), suggesting that our
281 observations were not due to a global defect in Rad51 loading *per se*, but rather an inability to
282 localise/stabilise Rad51 to stalled replication forks.

283 Conceivably, a defect in recruiting Rad51 to stalled forks may be due to either a failure to
284 properly load Rad51 onto ssDNA, or an inability to maintain loaded Rad51 on chromatin. To
285 investigate the former possibility, we examined the impact of BOD1L depletion on the recruitment
286 of BRCA1, BRCA2 and PALB2, which are essential for Rad51 loading to ICLs (Bhattacharyya *et*
287 *al*., 2000; Godthelp *et al*., 2006; Xia *et al*., 2007). Cells lacking BOD1L exhibited no observable
288 defects in the re-localisation of BRCA1, BRCA2 or GFP-PALB2 to foci following exposure to MMC
289 (**Figures 6H** and **S6G-I**), suggesting that BOD1L may instead be required to stabilise/retain Rad51
290 on damaged chromatin.

291 Proteins involved in Rad51 filament dissolution play a vital role in controlling HR and
292 maintaining genome stability. Of these, the RecQ-like helicases BLM and RECQL5, and the F-box-
293 containing helicase Fbh1 are the best studied: all three suppress Rad51-dependent HR,
294 particularly in response to replication stress. We speculated that the phenotypes observed in
295 BOD1L-deficient cells following MMC exposure may arise from the uncontrolled activity of one or
296 more of these anti-recombinase(s). We therefore siRNA-depleted BOD1L in combination with
297 BLM, Fbh1 or RECQL5, and monitored the levels of MMC-induced RPA S4/S8 phosphorylation
298 and Rad51 foci formation. Strikingly, loss of either Fbh1 or BLM (but not RECQL5) reduced MMC-
299 induced RPA S4/S8 phosphorylation and restored Rad51 focus formation in BOD1L-depleted cells
300 (**Figures 7A-B and S7A-C**). Consistent with this, co-depletion of Fbh1 in BOD1L-depleted cells
301 restored MMC-induced loading of Rad51 onto chromatin (**Figure S7D**). However, depletion of
302 Fbh1 or BLM was unable to restore Rad51 focus formation in the absence of BRCA2, suggesting
303 that BOD1L acts downstream of BRCA2 to control Rad51 (**Figure S7E**). Depleting Fbh1 or BLM
304 expression also partially alleviated the over-resection of stalled replication forks observed in cells
305 lacking BOD1L, in keeping with the notion that Rad51 suppresses aberrant fork resection.

306 Strikingly, RECQL5 depletion further increased fork resection in the absence of BOD1L, indicating
307 that these two factors act in separate pathways (**Figures 7C and S7F**). Lastly, ablating Fbh1 or
308 BLM expression also restored genome stability in cells depleted of BOD1L (**Figures 7D and S7G**).
309 Loss of RECQL5, however, had no restorative impact on MMC-induced chromosomal instability.
310 Finally, and in keeping with a role for BOD1L in stabilising Rad51 by counteracting BLM, both BLM
311 and Rad51 could be co-immunoprecipitated with BOD1L or CFlap-mBod1L (**Figure 7E and S7H**).
312 Taken together, these data demonstrate that BOD1L functions to restrain the pro-resection
313 and anti-recombinogenic functions of BLM/Fbh1 towards Rad51, thereby stabilising Rad51 on
314 chromatin and promoting HR-dependent repair of damaged replication forks. In the absence of
315 BOD1L, damaged replication forks undergo deleterious DNA2-dependent nucleolytic resection,
316 which compromises fork repair/restart and leads to catastrophic genome instability (**Figure 7F**).

DISCUSSION

The ability to efficiently resolve replication stress is vital to maintain genome stability. In this study, we have identified BOD1L as a factor associated with newly replicated chromatin that functions to prevent catastrophic DNA damage induced by replication stress by protecting damaged replication forks from promiscuous nucleolytic degradation.

Loss of Rad51-mediated fork protection underlies uncontrolled fork resection and genome instability in BOD1L deficient cells

Rad51-dependent HR plays an essential role to stabilise, protect and promote the restart of stalled or damaged replication forks. Central to this process is the BRCA1/BRCA2/PALB2-dependent loading of Rad51 onto RPA-coated ssDNA generated at such forks (Costanzo, 2011). Rad51 fork loading stabilises replication fork intermediates and prevents deleterious nucleolytic processing (Petermann *et al.*, 2010; Schlacher *et al.*, 2011; 2012). Loss of this protective activity cripples the repair/restart of damaged forks and compromises genomic integrity.

We observed that BOD1L depleted cells exhibit increased fork degradation in a manner comparable to BRCA1/BRCA2 deficient cells. This suggests that defects in the recruitment and/or stabilisation of Rad51 allow degradation of damaged forks in BOD1L-deficient cells. Yet, in marked contrast to the complete loss of BRCA2 or PALB2 (Yuan *et al.,* 1999; Xia *et al.,* 2006; Zhang *et al.,* 2009), loss of BOD1L does not impact on the recruitment of Rad51 to DSBs induced by IR. This implies that the function of BOD1L in regulating Rad51 in response to genotoxic damage is restricted to lesions that cause replication stress.

The repair and restart of forks requires the tightly regulated processing of replication damage (such as ICLs) by several different nucleases. Whilst such nucleolytic processing is important for cell survival, uncontrolled activity of these nucleases is also detrimental to genomic integrity (Adamo *et al*., 2010; Karanja *et al*., 2014). In keeping with this, uncontrolled resection of damaged forks and increased genomic instability observed in the absence of BOD1L was completely alleviated by co-depletion of DNA2. In contrast, inhibition of Mre11 activity with Mirin had no effect on the degradation of stalled replication forks in the absence of BOD1L. Since both BRCA2 and FANCD2 suppress the activity of Mre11 at stalled forks (Schlacher *et al.*, 2011; 2012;

346 Ying *et al.,* 2012), our data suggests that BOD1L acts independently to inhibit aberrant DNA2
347 activity. Based on this, loss of BOD1L and BRCA2 should further increase fork resection, rather
348 than exhibit the epistatic relationship we observed. Although the underlying reason is unclear, we
349 postulate that nucleolytic degradation of a damaged fork by one nuclease prohibits further
350 processing by other nucleases.

351 Interestingly, since BOD1L co-immunoprecipitated with both BRCA2 and FANCD2 in
352 unperturbed cells, this raises two intriguing possibilities: that multiple fork protection factors act to
353 individually block the activities of different nucleases towards replication forks, and that they may
354 exist in a single complex.

355

356 **Mechanisms for BOD1L in stabilising Rad51 on damaged chromatin**

357 Our data demonstrates that loss of BOD1L is epistatic with deficiencies in BRCA1/BRCA2,
358 although the phenotypes observed in the absence of BOD1L cannot be explained by an inability to
359 recruit BRCA1, BRCA2 or PALB2 to sites of replication stress. Instead, co-depletion of BOD1L with
360 the anti-recombinogenic helicases Fbh1 or BLM restored Rad51 focal recruitment, stalled
361 replication fork resection and genome stability. Thus, chromatin-bound Rad51 may be more
362 susceptible to anti-recombinases, and/or Rad51 nucleofilaments may be more unstable, in the
363 absence of BOD1L. Importantly, Fbh1 or BLM knockdown failed to recover MMC-induced Rad51
364 foci formation in BRCA2-depleted cells, suggesting that BOD1L acts downstream of
365 BRCA2/PALB2 (see **Figure S6F**). Moreover, BOD1L associates with Rad51, suggesting that it
366 may stabilise Rad51 directly. Together, our data suggest that BRCA2 and BOD1L function
367 independently in a common pathway to protect replication forks, and that BOD1L acts in a similar
368 manner to the C-terminus of BRCA2 (Esashi *et al*., 2007; Schlacher *et al*., 2011), i.e. promoting
369 Rad51 nucleofilament stability. Intriguingly, co-depletion of BOD1L with another anti-
370 recombinogenic helicase, RECQL5, failed to restore Rad51 foci formation, and actually
371 increased/accelerated fork degradation. This is in line with recent data demonstrating that the
372 combined loss of FA proteins with RECQL5 is additive in terms of fork degradation, and that BLM
373 and RECQL5 have divergent functions in the absence of an intact FA pathway (Kim *et al*., 2015).

374 It is unclear why depletion of two independent factors (namely BLM or Fbh1) is able to
375 compensate for a lack of BOD1L, although BLM and Fbh1 have partially redundant functions in
376 DT40 cells (Kohzaki *et al.*, 2007). Whilst Fbh1 and BLM both have pro- and anti-recombinogenic
377 activities (Bugreev *et al*., 2007; Fugger *et al*., 2009), BLM can displace Rad51 from ssDNA, and
378 can also potentiate HR through its ability to stimulate DNA2-dependent end-resection by binding to
379 RPA (Chen *et al*., 2013; Xue et al., 2013; Sturrzenegger *et al.,* 2014). It is possible that loss of
380 BLM activity in BOD1L/BLM knockdown cells has two effects: (1) increases Rad51 filament
381 stability and; (2) compromises DNA2-dependent resection of damaged forks, the latter of which
382 causes the genome instability apparent in BOD1L deficient cells.
383 Currently it is unknown whether BOD1L influences the activity of these anti-recombinases
384 directly or controls their access to the damaged replication fork and/or the Rad51 filament itself.
385 Given that BOD1L and BLM co-associate, it is tempting to speculate that BOD1L regulates BLM
386 activity directly. Alternatively, since the Rad51 paralogues stabilise Rad51 nucleofilaments by
387 blocking the translocase activities of anti-recombinogenic helicases (Amunugama *et al*., 2013; Liu
388 *et al.,* 2011), BOD1L may act in an analogous fashion to regulate access of BLM/Fbh1 to Rad51,
389 ultimately stabilising Rad51 nucleofilaments at damaged replication forks. As a consequence,
390 ablating BOD1L could promote uncontrolled BLM-DNA2-dependent resection, and allow
391 BLM/Fbh1-dependent dissolution of Rad51 filaments.
392
393 **BOD1L functions in the latter stages of the FA/HR pathway**
394 The phenotypic similarities between BOD1L-deficient cells and FA-defective cells,
395 particularly after ICL induction, suggest that BOD1L functions as part of the FA/HR pathway.
396 Indeed, loss of BOD1L and core/downstream FA components (namely FANCA and BRCA2) are
397 epistatic for MMC hypersensitivity and fork protection. In further support, the increased fork
398 resection apparent in both BOD1L-deficient and FANCD2-null cells is attributable to the nucleolytic
399 activity of DNA2 (Karanja *et al*., 2014). However, since BOD1L is not required for mono-
400 ubiquitylation or relocalisation of FANCD2 to sites of DNA damage, and also that the chromatin
401 localisation/retention of Rad51 is unaffected in cells lacking FA core components or FANCD2/I
402 (Ohashi *et al.,* 2005; Godthelp et al., 2006), this indicates that BOD1L functions in the latter stages

of the FA pathway, downstream of FANCD2/I. This also suggests that fork protection mechanisms independent of Rad51-loading (but perhaps dependent on Rad51 activity) also exist.

Increased origin firing contributes to genome instability in BOD1L deficient cells

We have shown that cells depleted of BOD1L exhibit increased new origin firing following the induction of replication stress. We hypothesise that this elevated origin firing is a cellular response to an inability to complete DNA replication, caused by the uncontrolled resection of stalled forks due to a failure to stabilise Rad51. This results in elevated levels of mitotic replication, UFBs, G1 53BP1 bodies and severe chromosomal instability.

Whether Rad51 defects alone promote new origin firing is currently unclear. Increased new origin firing does not occur in human cells depleted of Rad51 or in BRCA2-null CHO cells following HU (Petermann *et al.,* 2010; Jones *et al.*, 2014), but increased new origin firing has been shown in BLM-deficient cells and those lacking PALB2 (Davies *et al.*, 2007; Nikkila *et al.*, 2013). It therefore remains to be determined whether the inability of BOD1L-depleted cells to retain Rad51 at stalled replication forks contributes to the increase in origin firing. In spite of this, we predict that the increased origin firing in BOD1L deficient cells could contribute to genome instability, perhaps due to collisions between newly fired origins and damaged forks lying in close proximity.

Summary

Taken together, our data leads us to propose the following model (**Figure 7F**): BOD1L forms an essential component of the fork protection machinery. Upon stalling of a replication fork (for example by an ICL), limited nucleolytic resection allows Rad51-dependent HR and repair/restart of the stalled fork. BOD1L acts to stabilise Rad51 at such structures by protecting Rad51 nucleofilaments from the activities of Fbh1/BLM. In the absence of BOD1L, Rad51 is displaced from ssDNA by Fbh1/BLM, rendering the fork susceptible to uncontrolled resection by DNA2, and leading to catastrophic genome instability, in part mediated by the presence of under-replicated DNA.

EXPERIMENTAL PROCEDURES

Cell culture and generation of cell lines

A549, HeLa, HeLa S3, H1299 and HeLa-FUCCI cells were grown in Dulbecco's modified Eagle's medium supplemented with 10% fetal bovine serum (FBS) (Gibco) and penicillin/streptomycin. HeLa-CFlap-BOD1L and U-2-OS SUPER-RPA cells were cultivated as above in the presence of 200 μg/ml Geneticin. U-2-OS and U-2-OS-PALB2-GFP cells were cultured in McCoys 5A medium, supplemented with 10% FBS and penicillin/streptomycin. DT40 cells were cultured in RPMI 1640 medium (Invitrogen) supplemented with 7% FBS, 3% chicken serum, and 10 μM β-mercaptoethanol. Further details of DT40s, HeLa-CFlap-mBOD1L cells, siRNA transfections and clonogenic survival assays are given in the Extended Experimental Procedures.

iPOND

iPOND was performed on HeLa S3 as described previously (Sirbu *et al.,* 2013) with some modifications to allow for improved detection of high molecular weight proteins, which are described in Extended Experimental Procedures. In brief, newly synthesized DNA was labelled with 10μM EdU, cells were fixed in 1% formaldehyde, permeablised and the Click reaction was performed using Azide-PEG (3+3)-S-S-Biotin Conjugate (Click ChemistryTools). Following sonication, EdU labelled DNA was precipitated using Streptavidin beads and eluted in buffer containing DDT.

Statistical analyses

Differences in survival assays were analysed by two-way ANOVA. Statistical differences in all cases were determined by Student's t-test, except for fork asymmetry, which was analysed by Mann-Whitney rank sum test. In all cases: NS = $p>0.05$; * = $p<0.05$; ** = $p<0.01$; *** = $p<0.001$.

AUTHOR CONTRIBUTIONS

MRH, JJR and GSS designed the study, performed experiments and wrote the manuscript. AW performed iPOND. VB made HeLa-CFlap-mBOD1L cells and performed CFlap IPs. ANB and JN created BOD1L-null DT40s. ESM and AZ performed experiments and created reagents. ELR assisted with DNA combing. ND performed FISH. TS, SJB and WN supervised and advised on experiments. All authors contributed to manuscript revisions.

ACKNOWLEDGEMENTS

We are extremely grateful to Hongtao Yu, James Hsieh, Luis Toledo, Ross Warrington and Fumiko Esashi for valuable reagents. We thank Aga Gambus, Roger Grand, Eva Petermann and Malcolm Taylor for invaluable discussions. MRH, ESM and GSS are funded by a CR-UK Senior Fellowship (C17183/A13030). JJR is funded by the University of Birmingham and an MRC project grant (MR/M009882/1). AB, AW, JN and WN were funded by Worldwide Cancer Research and MRC Senior Non-Clinical Fellowships awarded to WN. AZ is funded by Worldwide Cancer Research (13-1012). ELR is funded by an MRC Ph.D. studentship. ND and TS are funded by a Leukemia and Lymphoma Research program grant (11045). VB is funded by the ERC and SJB is supported by the Wellcome Trust, CR-UK and ERC.

REFERENCES

Adamo, A., Collis, S.J., Adelman, C.A., Silva, N., Horejsi, Z., Ward, J.D., Martinez-Perez, E., Boulton, S.J., and La Volpe, A. (2010). Preventing nonhomologous end joining suppresses DNA repair defects of Fanconi anemia. Molecular cell 39, 25-35.

Akkari, Y.M., Bateman, R.L., Reifsteck, C.A., D'Andrea, A.D., Olson, S.B., and Grompe, M. (2001). The 4N cell cycle delay in Fanconi anemia reflects growth arrest in late S phase. Molecular genetics and metabolism 74, 403-412.

Amunugama, R., Groden, J., and Fishel, R. (2013). The HsRAD51B-HsRAD51C stabilizes the HsRAD51 nucleoprotein filament. DNA repair 12, 723-732.

Barlow, J.H., Faryabi, R.B., Callen, E., Wong, N., Malhowski, A., Chen, H.T., Gutierrez-Cruz, G., Sun, H.W., McKinnon, P., Wright, G., et al. (2013). Identification of early replicating fragile sites that contribute to genome instability. Cell 152, 620-632.

Bhattacharyya, A., Ear, U.S., Koller, B.H., Weichselbaum, R.R., and Bishop, D.K. (2000). The breast cancer susceptibility gene BRCA1 is required for subnuclear assembly of Rad51 and survival following treatment with the DNA cross-linking agent cisplatin. The Journal of biological chemistry 275, 23899-23903.

Bugreev, D.V., Yu, X., Egelman, E.H., and Mazin, A.V. (2007). Novel pro- and anti-recombination activities of the Bloom's syndrome helicase. Genes & development 21, 3085-3094.

Chan, K.L., North, P.S., and Hickson, I.D. (2007). BLM is required for faithful chromosome segregation and its localization defines a class of ultrafine anaphase bridges. The EMBO journal 26, 3397-3409.

Chan, K.L., Palmai-Pallag, T., Ying, S., and Hickson, I.D. (2009). Replication stress induces sister-chromatid bridging at fragile site loci in mitosis. Nature cell biology 11, 753-760.

Chen, H., Lisby, M., and Symington, L.S. (2013). RPA coordinates DNA end resection and prevents formation of DNA hairpins. Molecular cell 50, 589-600.

Conti, C., Seiler, J.A., and Pommier, Y. (2007). The mammalian DNA replication elongation checkpoint: implication of Chk1 and relationship with origin firing as determined by single DNA molecule and single cell analyses. Cell Cycle 6, 2760-2767.

Costanzo, V. (2011). Brca2, Rad51 and Mre11: performing balancing acts on replication forks. DNA repair 10, 1060-1065.

Davies, S.L., North, P.S., and Hickson, I.D. (2007). Role for BLM in replication-fork restart and suppression of origin firing after replicative stress. Nature structural & molecular biology 14, 677-679.

Durkin, S.G., and Glover, T.W. (2007). Chromosome fragile sites. Annual review of genetics 41, 169-192.

Esashi, F., Galkin, V.E., Yu, X., Egelman, E.H., and West, S.C. (2007). Stabilization of RAD51 nucleoprotein filaments by the C-terminal region of BRCA2. Nature Structural & Molecular Biology 14, 468-474.

Fugger, K., Mistrik, M., Danielsen, J.R., Dinant, C., Falck, J., Bartek, J., Lukas, J., and Mailand, N. (2009). Human Fbh1 helicase contributes to genome maintenance via pro- and anti-recombinase activities. The Journal of cell biology 186, 655-663.

530 Garaycoechea, J.I., and Patel, K.J. (2014). Why does the bone marrow fail in Fanconi anemia?
531 Blood 123, 26-34.
532
533 Gari, K., and Constantinou, A. (2009). The role of the Fanconi anemia network in the response to
534 DNA replication stress. Critical reviews in biochemistry and molecular biology 44, 292-325.
535
536 Godthelp, B.C., Wiegant, W.W., Waisfisz, Q., Medhurst, A.L., Arwert, F., Joenje, H., and
537 Zdzienicka, M.Z. (2006). Inducibility of nuclear Rad51 foci after DNA damage distinguishes all
538 Fanconi anemia complementation groups from D1/BRCA2. Mutation research 594, 39-48.
539
540 Heinrich, M.C., Hoatlin, M.E., Zigler, A.J., Silvey, K.V., Bakke, A.C., Keeble, W.W., Zhi, Y.,
541 Reifsteck, C.A., Grompe, M., Brown, M.G., et al. (1998). DNA cross-linker-induced G2/M arrest in
542 group C Fanconi anemia lymphoblasts reflects normal checkpoint function. Blood 91, 275-287.
543
544 Howlett, N.G., Taniguchi, T., Durkin, S.G., D'Andrea, A.D., and Glover, T.W. (2005). The Fanconi
545 anemia pathway is required for the DNA replication stress response and for the regulation of
546 common fragile site stability. Human molecular genetics 14, 693-701.
547
548 Jones, R.M., Kotsantis, P., Stewart, G.S., Groth, P., and Petermann, E. (2014). BRCA2 and
549 RAD51 promote double-strand break formation and cell death in response to gemcitabine.
550 Molecular cancer therapeutics 13, 2412-2421.
551
552 Karanja, K.K., Lee, E.H., Hendrickson, E.A., and Campbell, J.L. (2014). Preventing over-resection
553 by DNA2 helicase/nuclease suppresses repair defects in Fanconi anemia cells. Cell Cycle 13,
554 1540-1550.
555
556 Kim, T.M., Son, M.Y., Dodds, S., Hu, L., Luo, G., and Hasty, P. (2015). RECQL5 and BLM exhibit
557 divergent functions in cells defective for the Fanconi anemia pathway. Nucleic Acids Research 43,
558 893-903.

559

560 Kohzaki, M., Hatanaka, A., Sonoda, E., Yamazoe, M., Kikuchi, K., Vu Trung, N., Szuts, D., Sale,
561 J.E., Shinagawa, H., Watanabe, M., et al. (2007). Cooperative roles of vertebrate Fbh1 and Blm
562 DNA helicases in avoidance of crossovers during recombination initiated by replication fork
563 collapse. Molecular and cellular biology 27, 2812-2820.

564

565 Koundrioukoff, S., Carignon, S., Techer, H., Letessier, A., Brison, O., and Debatisse, M. (2013).
566 Stepwise activation of the ATR signaling pathway upon increasing replication stress impacts fragile
567 site integrity. PLoS genetics 9, e1003643.

568

569

570 Liu, J., Renault, L., Veaute, X., Fabre, F., Stahlberg, H., and Heyer, W.D. (2011). Rad51
571 paralogues Rad55-Rad57 balance the antirecombinase Srs2 in Rad51 filament formation. Nature
572 479, 245-248.

573

574 Lukas, C., Savic, V., Bekker-Jensen, S., Doil, C., Neumann, B., Pedersen, R.S., Grofte, M., Chan,
575 K.L., Hickson, I.D., Bartek, J., et al. (2011). 53BP1 nuclear bodies form around DNA lesions
576 generated by mitotic transmission of chromosomes under replication stress. Nature cell biology 13,
577 243-253.

578

579 Matsuoka, S., Ballif, B.A., Smogorzewska, A., McDonald, E.R., 3rd, Hurov, K.E., Luo, J.,
580 Bakalarski, C.E., Zhao, Z., Solimini, N., Lerenthal, Y., et al. (2007). ATM and ATR substrate
581 analysis reveals extensive protein networks responsive to DNA damage. Science 316, 1160-1166.

582

583 Naim, V., and Rosselli, F. (2009a). The FANC pathway and BLM collaborate during mitosis to
584 prevent micro-nucleation and chromosome abnormalities. Nature cell biology 11, 761-768.

585

586 Naim, V., and Rosselli, F. (2009b). The FANC pathway and mitosis: a replication legacy. Cell
587 Cycle 8, 2907-2911.

588

589 Nikkila, J., Parplys, A.C., Pylkas, K., Bose, M., Huo, Y., Borgmann, K., Rapakko, K., Nieminen, P.,
590 Xia, B., Pospiech, H., et al. (2013). Heterozygous mutations in PALB2 cause DNA replication and
591 damage response defects. Nature communications 4, 2578.

592

593 Ohashi, A., Zdzienicka, M.Z., Chen, J., and Couch, F.J. (2005). Fanconi anemia complementation
594 group D2 (FANCD2) functions independently of BRCA2- and RAD51-associated homologous
595 recombination in response to DNA damage. The Journal of biological chemistry 280, 14877-14883.

596

597 Petermann, E., Orta, M.L., Issaeva, N., Schultz, N., and Helleday, T. (2010). Hydroxyurea-stalled
598 replication forks become progressively inactivated and require two different RAD51-mediated
599 pathways for restart and repair. Molecular cell 37, 492-502.

600

601 Porter, I.M., McClelland, S.E., Khoudoli, G.A., Hunter, C.J., Andersen, J.S., McAinsh, A.D., Blow,
602 J.J., and Swedlow, J.R. (2007). Bod1, a novel kinetochore protein required for chromosome
603 biorientation. The Journal of cell biology 179, 187-197.

604

605 Porter, I.M., Schleicher, K., Porter, M., and Swedlow, J.R. (2013). Bod1 regulates protein
606 phosphatase 2A at mitotic kinetochores. Nature communications 4, 2677.

607

608 Rodriguez-Lopez, A.M., Jackson, D.A., Iborra, F., and Cox, L.S. (2002). Asymmetry of DNA
609 replication fork progression in Werner's syndrome. Aging cell 1, 30-39.

610

611 Schlacher, K., Christ, N., Siaud, N., Egashira, A., Wu, H., and Jasin, M. (2011). Double-strand
612 break repair-independent role for BRCA2 in blocking stalled replication fork degradation by
613 MRE11. Cell 145, 529-542.

614

615 Schlacher, K., Wu, H., and Jasin, M. (2012). A distinct replication fork protection pathway connects
616 Fanconi anemia tumor suppressors to RAD51-BRCA1/2. Cancer cell 22, 106-116.

Schoder, C., Liehr, T., Velleuer, E., Wilhelm, K., Blaurock, N., Weise, A., and Mrasek, K. (2010). New aspects on chromosomal instability: chromosomal break-points in Fanconi anemia patients co-localize on the molecular level with fragile sites. International journal of oncology 36, 307-312.

Sirbu, B.M., McDonald, W.H., Dungrawala, H., Badu-Nkansah, A., Kavanaugh, G.M., Chen, Y., Tabb, D.L., and Cortez, D. (2013). Identification of proteins at active, stalled, and collapsed replication forks using isolation of proteins on nascent DNA (iPOND) coupled with mass spectrometry. The Journal of biological chemistry 288, 31458-31467.

Smogorzewska, A., Matsuoka, S., Vinciguerra, P., McDonald, E.R., 3rd, Hurov, K.E., Luo, J., Ballif, B.A., Gygi, S.P., Hofmann, K., D'Andrea, A.D., et al. (2007). Identification of the FANCI protein, a monoubiquitinated FANCD2 paralog required for DNA repair. Cell 129, 289-301.

Sturzenegger, A., Burdova, K., Kanagaraj, R., Levikova, M., Pinto, C., Cejka, P., and Janscak, P. (2014). DNA2 cooperates with the WRN and BLM RecQ helicases to mediate long-range DNA end resection in human cells. The Journal of biological chemistry 289, 27314-27326.

Toledo, L.I., Altmeyer, M., Rask, M.B., Lukas, C., Larsen, D.H., Povlsen, L.K., Bekker-Jensen, S., Mailand, N., Bartek, J., and Lukas, J. (2013). ATR prohibits replication catastrophe by preventing global exhaustion of RPA. Cell 155, 1088-1103.

Walden, H., and Deans, A.J. (2014). The Fanconi anemia DNA repair pathway: structural and functional insights into a complex disorder. Annual review of biophysics 43, 257-278.

Xia, B., Dorsman, J.C., Ameziane, N., de Vries, Y., Rooimans, M.A., Sheng, Q., Pals, G., Errami, A., Gluckman, E., Llera, J., et al. (2007). Fanconi anemia is associated with a defect in the BRCA2 partner PALB2. Nature genetics 39, 159-161.

Xia, B., Sheng, Q., Nakanishi, K., Ohashi, A., Wu, J., Christ, N., Liu, X., Jasin, M., Couch, F.J., and Livingston, D.M. (2006). Control of BRCA2 cellular and clinical functions by a nuclear partner, PALB2. Molecular cell 22, 719-729.

Xue, X., Raynard, S., Busygina, V., Singh, A.K., and Sung, P. (2013). Role of replication protein A in double holliday junction dissolution mediated by the BLM-Topo IIIalpha-RMI1-RMI2 protein complex. The Journal of biological chemistry 288, 14221-14227.

Ying, S., Hamdy, F.C., and Helleday, T. (2012). Mre11-dependent degradation of stalled DNA replication forks is prevented by BRCA2 and PARP1. Cancer Research 72, 2814-2821.

Yuan, S.S., Lee, S.Y., Chen, G., Song, M., Tomlinson, G.E., and Lee, E.Y. (1999). BRCA2 is required for ionizing radiation-induced assembly of Rad51 complex in vivo. Cancer research 59, 3547-3551.

Zeman, M.K., and Cimprich, K.A. (2014). Causes and consequences of replication stress. Nature cell biology 16, 2-9.

Zhang, F., Fan, Q., Ren, K., and Andreassen, P.R. (2009). PALB2 functionally connects the breast cancer susceptibility proteins BRCA1 and BRCA2. Molecular cancer research : MCR 7, 1110-1118.

FIGURE LEGENDS

Figure 1: BOD1L is present at newly-replicated DNA, and ensures cellular viability after replication stress. (A) *Upper:* Schematic of human BOD1L and BOD1 domain structure and ATM/ATR phosphorylation sites. *Lower:* Amino acid sequence alignment of BOD1L and BOD1. Conserved residues (red) and similar residues (+) are denoted. **(B)** Immunoblotting of EdU-coprecipitates from HeLa S3 cells. **(C-D)** HeLa cells were transfected with the indicated siRNAs, and pulsed with 10 μM EdU for 10 minutes before pre-extraction/fixation. EdU incorporation was visualised with Click-iT chemistry, and detection of protein-protein associations were performed using a fluorescently labelled PLA probe along with the indicated antibodies. (C) shows quantification of PLA signals/nucleus from at least 100 cells (n = 3; lines denote mean values), and representative images are shown (D). Scale bars = 10 μm. **(E)** HeLa nuclear cell extracts were subjected to IP with the indicated antibodies, and inputs and immunoprecipitates were analyzed by immunoblotting. Blots originate from a single gel. A white line denotes removal of irrelevant lanes. **(F)** The survival of HeLa cells transfected with the indicated siRNA following exposure to mitomycin C (MMC) or hydroxyurea (HU) was assessed by colony survival assay. **(G)** Micronuclei formation following DNA damage was assessed in siRNA-transfected HeLa cells by fluorescence microscopy. Plots (F)-(G) represent mean data from four independent experiments; error bars = SEM. See also Figure S1.

Figure 2: BOD1L is functionally distinct from BOD1. (A). Whole cell extracts (WCE) of HeLa cells transfected with the indicated siRNA were analysed by immunoblotting after exposure to 50 ng/ml MMC for the denoted times. **(B)** HeLa cells from (A) were exposed to 50 ng/ml MMC for 24 h, and micronuclei enumerated. **(C-D)** The survival of HeLa cells transfected with the indicated siRNA was assessed by colony survival assay as in **Figure 1F**. **(E-F)** Untreated HeLa cells from (A) were immunostained with antibodies to α-tubulin and PCNT1, and the percentage of mitotic cells in each stage of mitosis (E), or their ability to form centrosomes (F), was analysed by immunofluorescence. Scale bars = 10 μm. Data represent mean ± SEM of three independent experiments.

Figure 3: BOD1L knockdown leads to problematic resolution of replication stress. (A) The percentage of micronuclei positive for either 53BP1 or CENPA was quantified by immunofluorescence microscopy in HeLa cells transfected with indicated siRNAs after exposure to 50 ng/ml MMC for 24 h. **(B)** The percentage of mitotic cells with PICH-positive UFBs was quantified in transfected HeLa cells after exposure to 250 ng/ml MMC for 3 h and release into fresh media for 36 h. **(C)** The mean percentage of PICH-positive UFBs with terminal FANCD2 foci in mitotic cells from (B) is indicated. **(D)** Cells from (B) were pulsed with 10 μM EdU for 45 minutes before fixation. Mitotic EdU incorporation was visualised with Click chemistry labelling, and the mean number of EdU foci per mitotic cell, and merged representative images, are shown. Scale bars = 10 μm. **(E-F)** HeLa-FUCCI cells were siRNA-transfected, and exposed to 50 ng/ml MMC for 24 h. (E) WCE were analysed by immunoblotting. Loading control denotes a non-specific protein detected by anti-BOD1L antibody. (F) The number of 53BP1 bodies in RFP-positive (i.e. G1) cells was enumerated. **(G)** Damage to metaphase chromosomes from HeLa cells subjected to the indicated siRNAs was determined by Geimsa staining and light microscopy. *Upper:* Graphs integrate data from three independent experiments (n = 150; lines denote mean values). *Lower:* Representative metaphase spreads are shown, with chromosomal damage denoted by arrowheads. **(H)** Cells from (G) were analysed by FISH using probes against FRA16D. Plots represent mean ± SEM of three independent experiments. See also Figure S2.

Figure 4: BOD1L knockdown increases origin firing after replication stress and destabilises replication forks. (A-B) The cell cycle profiles of HeLa cells subjected to the indicated siRNAs were analysed by flow cytometry. Representative profiles from untreated cells (A) or after exposure to 250 ng/ml MMC for 3 h (B) are shown. **(C-D)** DNA fibre analysis of HeLa cells transfected with the indicated siRNAs. Cells were pulsed with CldU, exposed to 2 mM HU for 2 h, and pulsed with IdU. Plots indicate ratios of left/right fork lengths of bidirectional replication forks travelling from a single origin. Lines denote median ratios (C). DNA fibres were enumerated, and the percentage of new origins (IdU-labelled only) is displayed (D). **(E)** Transfected cells from (C) were exposed to 50 ng/ml MMC for 24 h, and pulsed sequentially with CldU and IdU. DNA fibres were quantified, and the percentage of new origins is displayed. **(F)** WCE of HeLa cells transfected as above and

exposed to MMC for the indicated times were analysed by immunoblotting. *Chronic = 50 ng/ml MMC. **Acute = 250 ng/ml MMC for 3h followed by wash out. Times for acute exposure indicate h post washout. Plots represent mean ± SEM of at least three independent experiments. See also Figure S3.

Figure 5: BOD1L prevents excessive ssDNA formation and RPA2 hyper-phosphorylation after MMC exposure. (A) Soluble and chromatin fractions of U-2-OS cells transfected with the indicated siRNAs, and exposed to 100 ng/ml MMC for 24 h, were analysed by immunoblotting. Loading control denotes a non-specific protein detected by anti-BOD1L antibody. Blots originate from a single gel. A white line denotes removal of superfluous lanes. **(B)** RPA foci formation was analysed in HeLa cells transfected as above and exposed to 50 ng/ml MMC for the denoted times. **(C)** Native BrdU foci formation in U-2-OS cells by fluorescence microscopy. Cells were transfected with the indicated siRNAs, and BrdU added for 24 h. Cells were exposed to 50 ng/ml MMC for a further 24 h in the presence of BrdU, and immunostained with antibodies to BrdU and γH2AX. Foci formation was analysed (see **Figure S4B**), and enumerated. **(D)** WCE of HeLa cells transfected as in (B), and exposed to MMC for the indicated times, were analysed by immunoblotting. *Chronic = 50 ng/ml MMC. **Acute = 250 ng/ml MMC for 3h followed by wash out. Times for acute exposure indicate h post washout. **(E)** Phospho-RPA (S4/S8) and RPA foci formation in transfected HeLa cells exposed to 50 ng/ml MMC for 24 h. **(F)** The number of double positive cells from (E) was enumerated. **(G)** Detection of protein-protein interactions was performed using a fluorescently labelled PLA probe in HeLa cells from (B). The plot shows quantification of PLA signals/nucleus from at least 100 cells (n=3; lines denote mean values), and representative images are shown. Plots represent mean ± SEM of three independent experiments. Scale bars = 10 μm. See also Figure S4.

Figure 6: BOD1L is required to suppress aberrant fork resection after replication stress, and is required for efficient Rad51 chromatin loading. (A) Fork degradation was analysed in U-2-OS cells. Cells were transfected with the indicated siRNAs, pulsed for 20 min each with CldU and

IdU, and exposed to 4 mM HU for 5 h. DNA was visualised with antibodies to CldU and IdU, and plots denote the average ratios of IdU:CldU label lengths from three independent experiments. Arrows indicate mean values (see **Figure S5B**). **(B)** HeLa nuclear cell extracts were subjected to IP with the denoted antibodies, and inputs and immunoprecipitates were analyzed by immunoblotting. Blots originate from a single gel. A white line denotes removal of irrelevant lanes. **(C)** Fork degradation in U-2-OS cells transfected and treated as in (A) was analysed. Where appropriate cells were treated with Mirin for the duration of the HU pulse (see **Figure S5H**). **(D)** Micronuclei formation was quantified in HeLa cells transfected with the indicated siRNAs and treated with 50 ng/ml MMC for 24 h. **(E)** Damage to metaphase chromosomes from cells (D) was analysed (n = 150; lines denote mean values). **(F)** Rad51 foci formation was analysed in siRNA-transfected HeLa cells, and exposed to 50 ng/ml MMC for the indicated times. Scale bars = 10 μm. **(G)** Soluble and chromatin fractions from **Figure 5A** were analysed by immunoblotting. **(H)** Foci formation of BRCA1 and BRCA2 was analysed in HeLa cells from (F). Alternatively, U-2-OS-PALB2-GFP cells were transfected with the indicated siRNAs, exposed to 50 ng/ml MMC for 24 h, and fixed. In both cases mean percentage of cells with foci are shown (see **Figures S6G-I**). Plots (D-H) represent mean ± SEM of three independent experiments. See also Figures S5 and S6.

Figure 7: BOD1L stabilises Rad51 chromatin loading to prevent excessive replication fork resection. (A-B) RPA2/phospho-RPA2 S4/S8 (A) or Rad51 (B) foci formation was analysed in HeLa cells transfected with the indicated siRNAs and exposed to 50 ng/ml MMC for 24 h. Scale bars = 10 μm. **(C)** Fork degradation was assessed in U-2-OS cells transfected with the indicated siRNAs as described in **Figure 6A** (see also **Figure S7F**). **(D)** Damage to metaphase chromosomes in HeLa cells from (A) was analysed (n = 100; lines denote mean values). **(E)** HeLa nuclear cell extracts subjected to IP with the indicated antibodies, and inputs and immunoprecipitates were analyzed by immunoblotting. Blots originate from a single gel. A white line denotes removal of irrelevant lanes. Plots (C-D) represent mean ± SEM of three independent experiments. **(F)** Model of BOD1L function to promote Rad51 nucleofilament stability and prevent uncontrolled resection of replication forks. Upon replication fork stalling, forks undergo minimal nucleolytic processing (i), allowing Rad51 loading/protection by BRCA1/BRCA2/PALB2 (ii). BOD1L

784 acts to stabilise Rad51 nucleofilaments by protecting them from the activities of BLM/Fbh1 (iii),
785 thus preventing uncontrolled resection and allowing Rad51-mediated repair/restart of forks,
786 ultimately maintaining genome stability. In the absence of BOD1L, BLM/Fbh1 act to remove Rad51
787 from such forks exposing them to uncontrolled DNA2-dependent processing (iv). To compensate
788 for this fork instability, increased new origin firing occurs. When combined with uncontrolled
789 resection of replication forks, this leads to catastrophic genome instability (v). See also Figure S7.

Figure 1

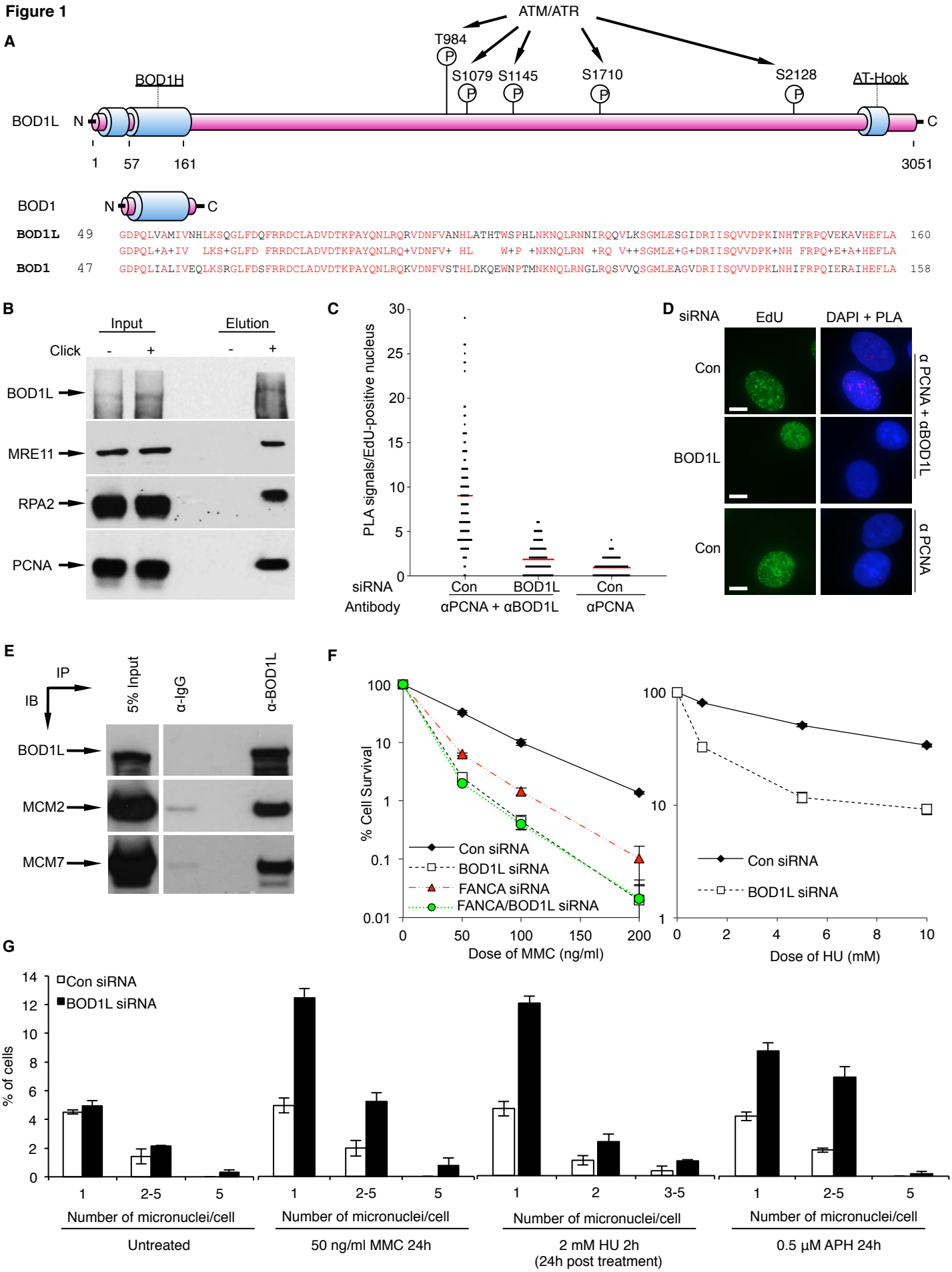
A
ATM/ATR
T984
S1079
S1145
S1710
S2128
AT-Hook
BOD1H
BOD1L
N
C
1
57
161
3051
BOD1
BOD1L 49 GDPQLVAMIVNHLKSQGLFDQFRRDCLADVDTKPAYQNLRQRVDNFVANHLATHTWSPHLNKNQLRNNIRQQVLKSGMLESGIDRIISQVVDPKINHTFRPQVEKAVHEFLA 160
GDPQL+A+IV LKS+GLFD FRRDCLADVDTKPAYQNLRQ+VDNFV+ HL W+P +NKNQLRN +RQ V++SGMLE+G+DRIISQVVDPK+NH FRPQ+E+A+HEFLA
BOD1 47 GDPQLIALIVEQLKSRGLFDSFRRDCLADVDTKPAYQNLRQKVDNFVSTHLDKQEWNPTMNKNQLRNGLRQSVVQSGMLEAGVDRIISQVVDPKLNHIFRPQIERAIHEFLA 158
B
Input
Elution
Click
-
+
-
+
BOD1L
MRE11
RPA2
PCNA
C
PLA signals/EdU-positive nucleus
siRNA
Con
BOD1L
Con
Antibody
αPCNA + αBOD1L
αPCNA
D
siRNA
EdU
DAPI + PLA
Con
BOD1L
Con
α PCNA + αBOD1L
α PCNA
E
IP
IB
5% Input
α-IgG
α-BOD1L
BOD1L
MCM2
MCM7
F
% Cell Survival
Con siRNA
BOD1L siRNA
FANCA siRNA
FANCA/BOD1L siRNA
Dose of MMC (ng/ml)
Dose of HU (mM)
G
Con siRNA
BOD1L siRNA
% of cells
Number of micronuclei/cell
Untreated
50 ng/ml MMC 24h
2 mM HU 2h
(24h post treatment)
0.5 μM APH 24h

Figure 2

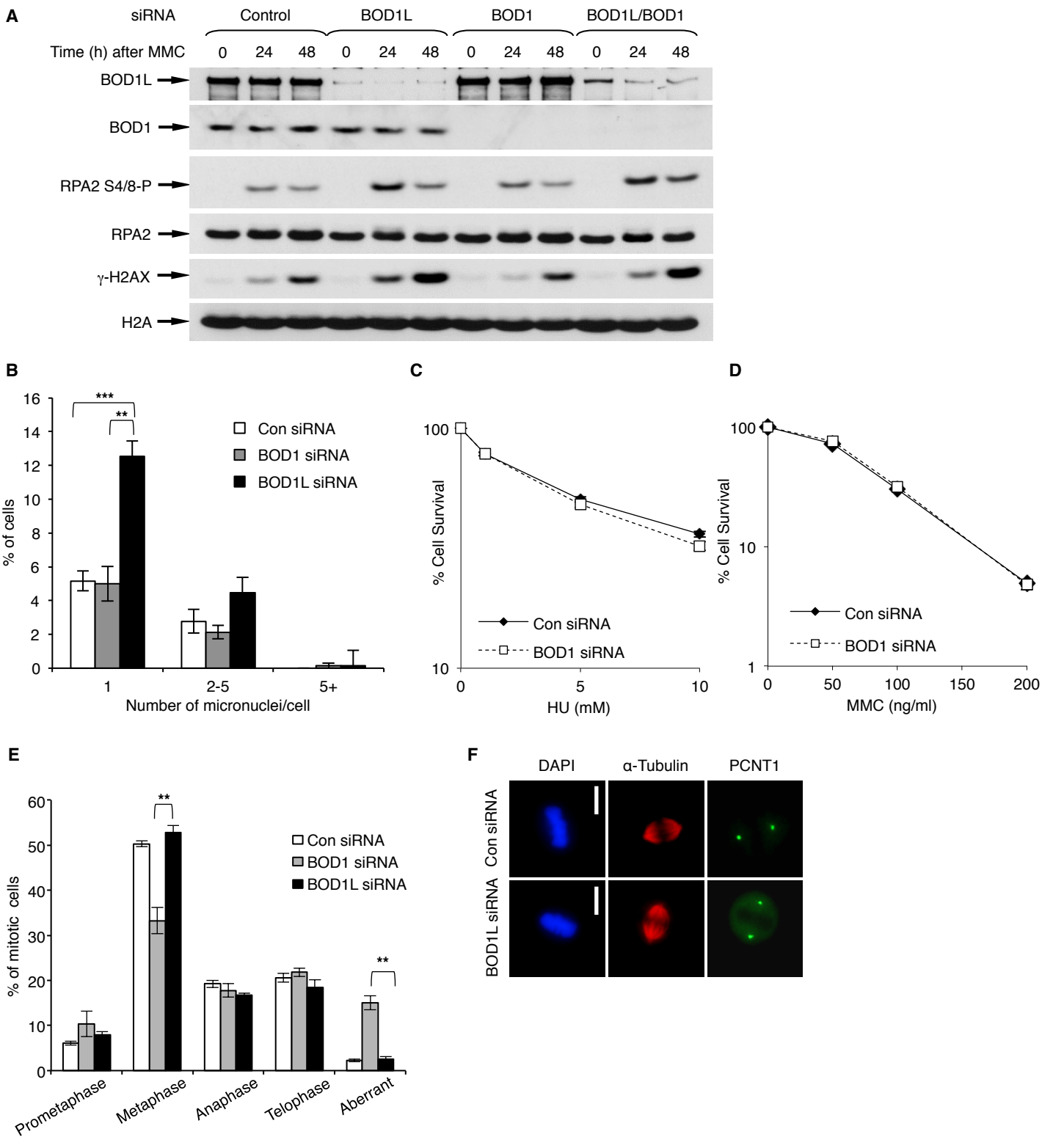
A
siRNA
Control
BOD1L
BOD1
BOD1L/BOD1
Time (h) after MMC
0 24 48 0 24 48 0 24 48 0 24 48
BOD1L
BOD1
RPA2 S4/8-P
RPA2
γ-H2AX
H2A
B
% of cells
Number of micronuclei/cell
1
2-5
5+
Con siRNA
BOD1 siRNA
BOD1L siRNA
***
**
C
% Cell Survival
HU (mM)
Con siRNA
BOD1 siRNA
D
% Cell Survival
MMC (ng/ml)
Con siRNA
BOD1 siRNA
E
% of mitotic cells
Prometaphase
Metaphase
Anaphase
Telophase
Aberrant
Con siRNA
BOD1 siRNA
BOD1L siRNA
F
DAPI
α-Tubulin
PCNT1
Con siRNA
BOD1L siRNA

Figure 3

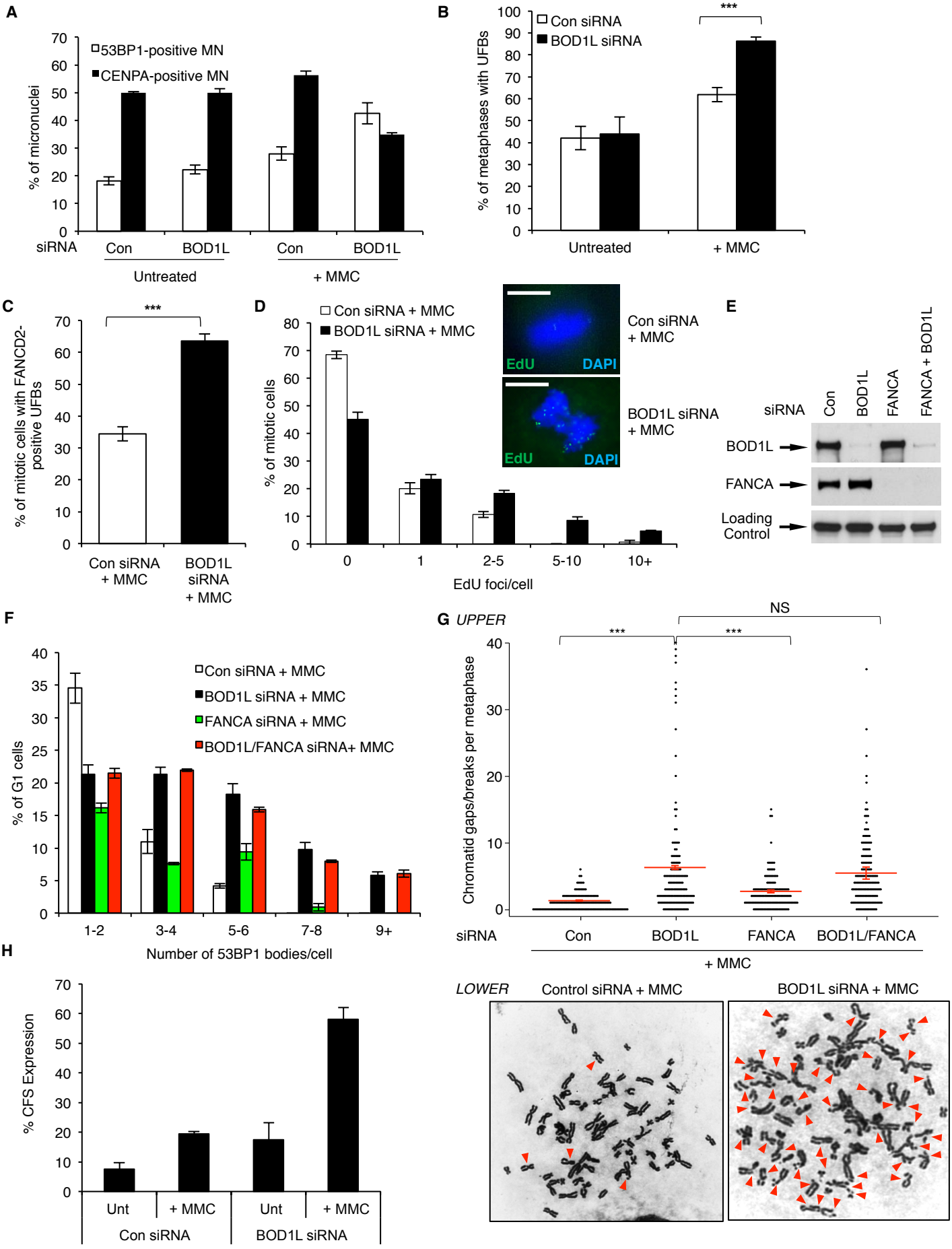
A
% of micronuclei
53BP1-positive MN
CENPA-positive MN
siRNA
Con
BOD1L
Con
BOD1L
Untreated
+ MMC
B
% of metaphases with UFBs
Con siRNA
BOD1L siRNA
***
Untreated
+ MMC
C
% of mitotic cells with FANCD2-positive UFBs
***
Con siRNA + MMC
BOD1L siRNA + MMC
D
% of mitotic cells
Con siRNA + MMC
BOD1L siRNA + MMC
EdU
DAPI
Con siRNA + MMC
BOD1L siRNA + MMC
0
1
2-5
5-10
10+
EdU foci/cell
E
siRNA
Con
BOD1L
FANCA
FANCA + BOD1L
BOD1L
FANCA
Loading Control
F
% of G1 cells
Con siRNA + MMC
BOD1L siRNA + MMC
FANCA siRNA + MMC
BOD1L/FANCA siRNA+ MMC
1-2
3-4
5-6
7-8
9+
Number of 53BP1 bodies/cell
G UPPER
NS
***
***
Chromatid gaps/breaks per metaphase
siRNA
Con
BOD1L
FANCA
BOD1L/FANCA
+ MMC
H
% CFS Expression
Unt
+ MMC
Unt
+ MMC
Con siRNA
BOD1L siRNA
LOWER
Control siRNA + MMC
BOD1L siRNA + MMC

Figure 4

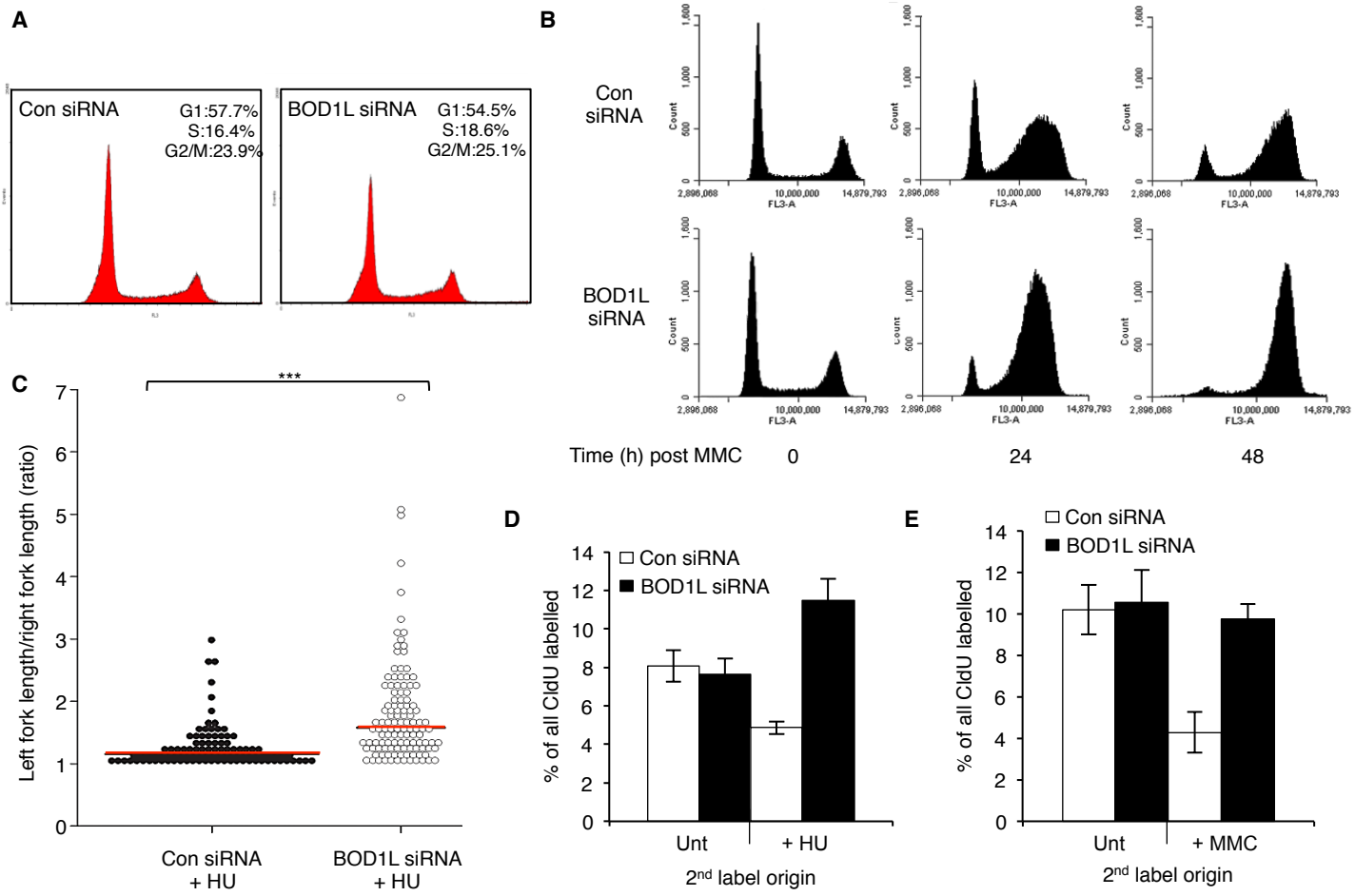
A
Con siRNA
G1:57.7%
S:16.4%
G2/M:23.9%
BOD1L siRNA
G1:54.5%
S:18.6%
G2/M:25.1%
B
Con siRNA
BOD1L siRNA
Count
FL3-A
Time (h) post MMC
0
24
48
C
***
Left fork length/right fork length (ratio)
Con siRNA + HU
BOD1L siRNA + HU
D
Con siRNA
BOD1L siRNA
% of all CldU labelled
Unt
+ HU
2nd label origin
E
Con siRNA
BOD1L siRNA
% of all CldU labelled
Unt
+ MMC
2nd label origin

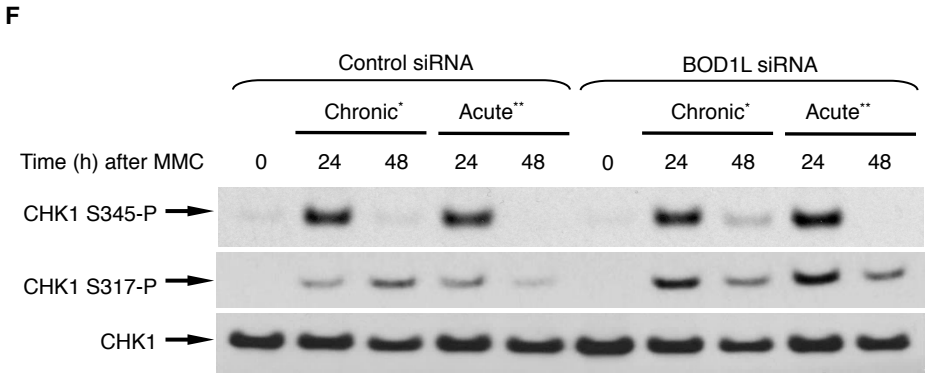
F
Control siRNA
BOD1L siRNA
Chronic*
Acute**
Time (h) after MMC
0
24
48
24
48
0
24
48
24
48
CHK1 S345-P
CHK1 S317-P
CHK1

Figure 5

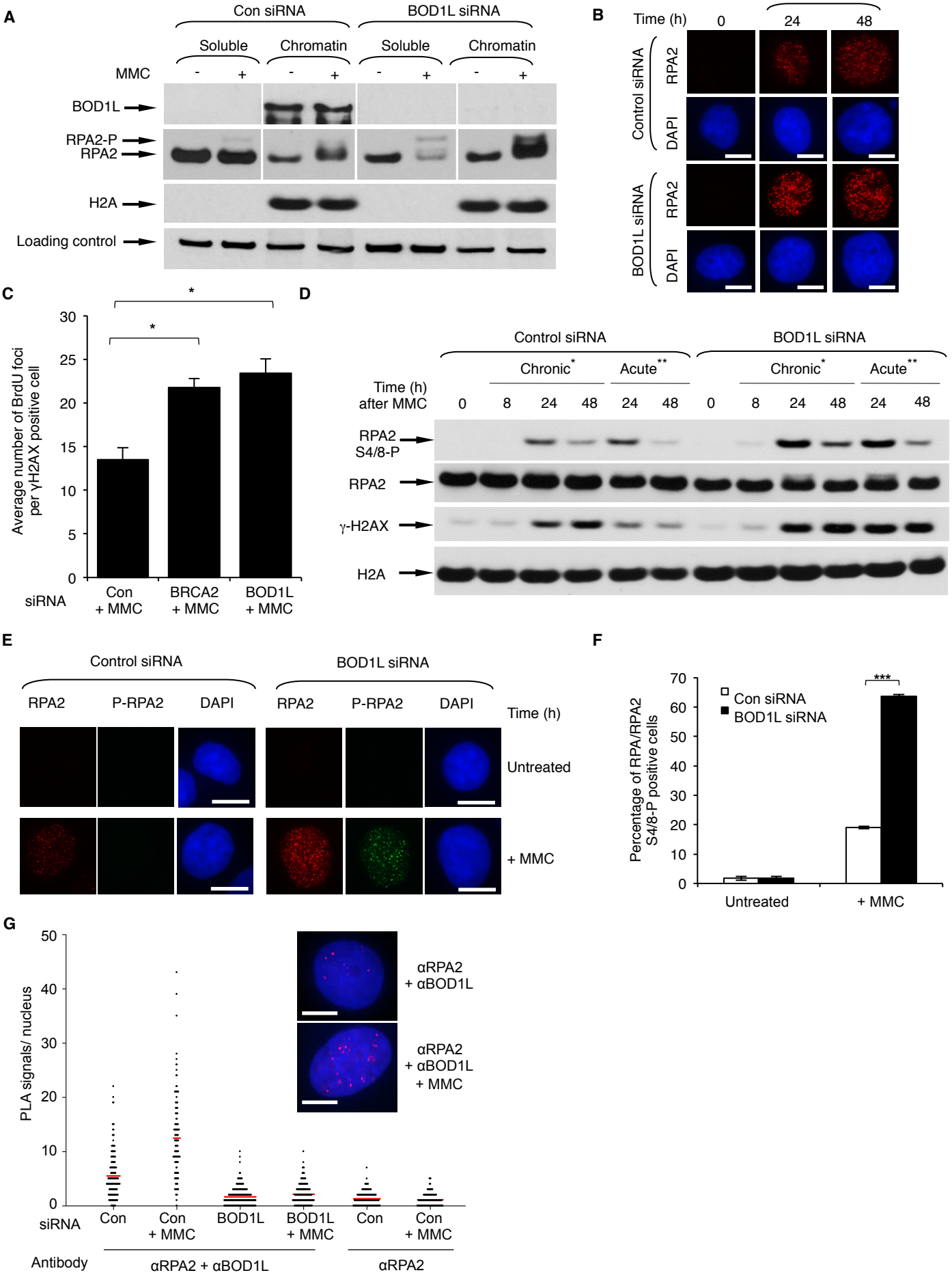
A
Con siRNA
BOD1L siRNA
Soluble
Chromatin
Soluble
Chromatin
MMC
- + - + - + - +
BOD1L
RPA2-P
RPA2
H2A
Loading control
B
+ MMC
Time (h)
0
24
48
Control siRNA
RPA2
DAPI
BOD1L siRNA
RPA2
DAPI
C
Average number of BrdU foci per γH2AX positive cell
30
25
20
15
10
5
0
*
*
siRNA
Con + MMC
BRCA2 + MMC
BOD1L + MMC
D
Control siRNA
BOD1L siRNA
Chronic*
Acute**
Chronic*
Acute**
Time (h) after MMC
0 8 24 48 24 48 0 8 24 48 24 48
RPA2 S4/8-P
RPA2
γ-H2AX
H2A
E
Control siRNA
BOD1L siRNA
RPA2
P-RPA2
DAPI
RPA2
P-RPA2
DAPI
Time (h)
Untreated
+ MMC
F
Percentage of RPA/RPA2 S4/8-P positive cells
70
60
50
40
30
20
10
0
Con siRNA
BOD1L siRNA
***
Untreated
+ MMC
G
PLA signals/ nucleus
50
40
30
20
10
0
αRPA2 + αBOD1L
αRPA2 + αBOD1L + MMC
siRNA
Con
Con + MMC
BOD1L
BOD1L + MMC
Con
Con + MMC
Antibody
αRPA2 + αBOD1L
αRPA2

Figure 6

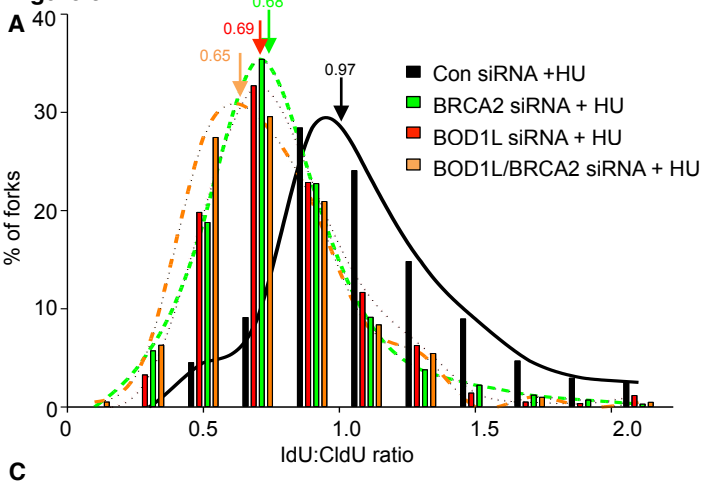
A
0.68
0.69
0.65
0.97
Con siRNA +HU
BRCA2 siRNA + HU
BOD1L siRNA + HU
BOD1L/BRCA2 siRNA + HU
% of forks
IdU:CldU ratio

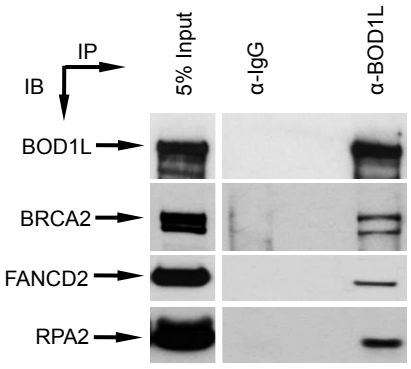
B
IP
IB
5% Input
α-IgG
α-BOD1L
BOD1L
BRCA2
FANCD2
RPA2

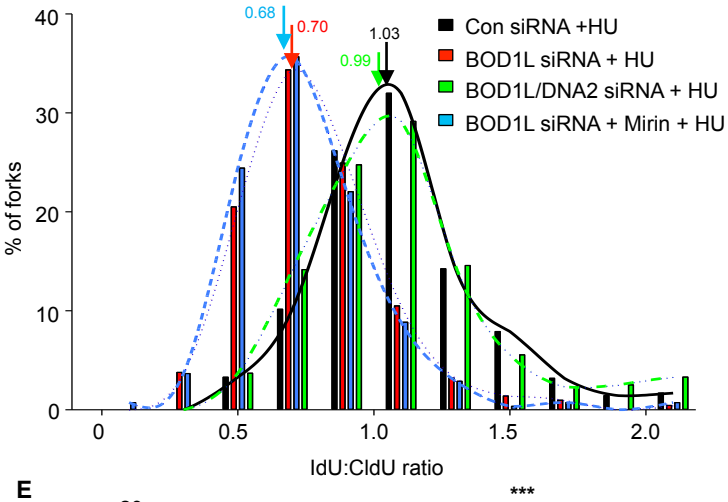
C
0.68
0.70
1.03
0.99
Con siRNA +HU
BOD1L siRNA + HU
BOD1L/DNA2 siRNA + HU
BOD1L siRNA + Mirin + HU
% of forks
IdU:CldU ratio

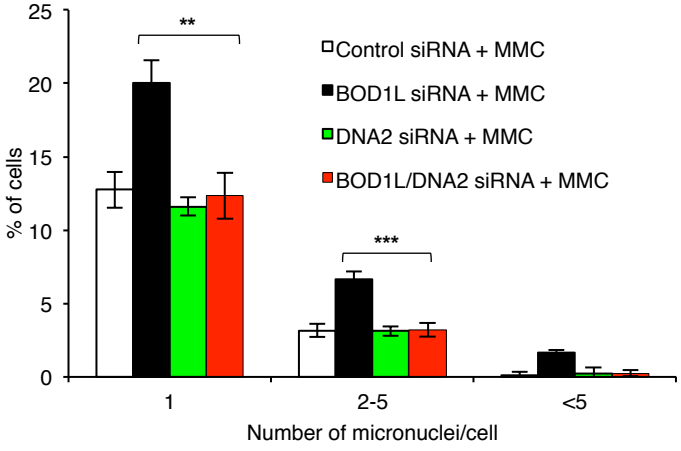
D
**
***
Control siRNA + MMC
BOD1L siRNA + MMC
DNA2 siRNA + MMC
BOD1L/DNA2 siRNA + MMC
% of cells
1
2-5
<5
Number of micronuclei/cell

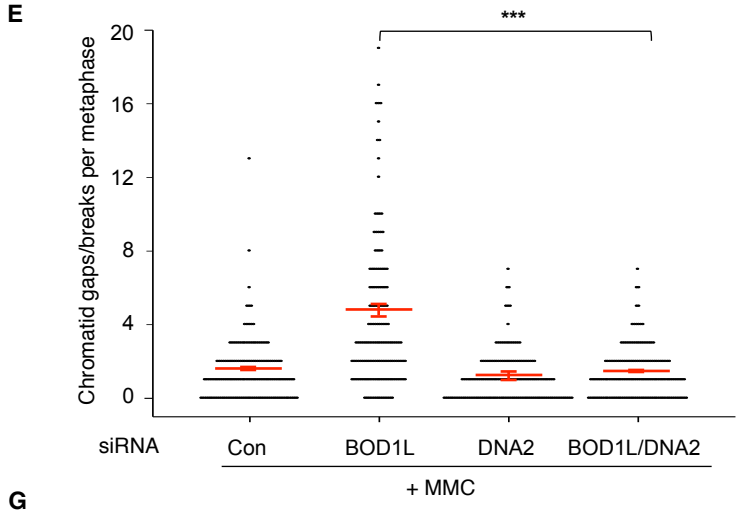
E
***
Chromatid gaps/breaks per metaphase
siRNA
Con
BOD1L
DNA2
BOD1L/DNA2
+ MMC

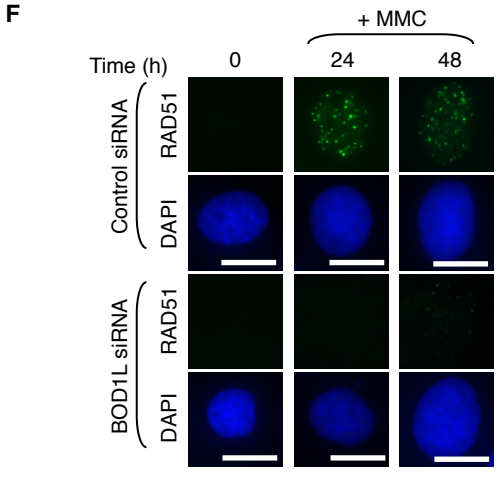
F
+ MMC
Time (h)
0
24
48
Control siRNA
BOD1L siRNA
RAD51
DAPI

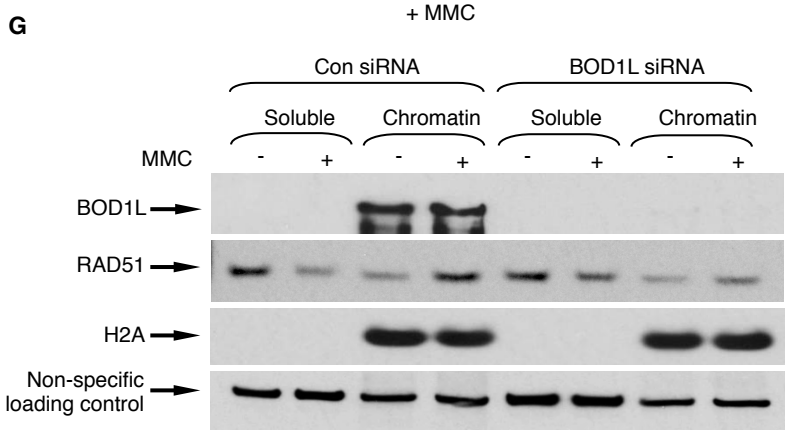
G
Con siRNA
BOD1L siRNA
Soluble
Chromatin
MMC
BOD1L
RAD51
H2A
Non-specific loading control

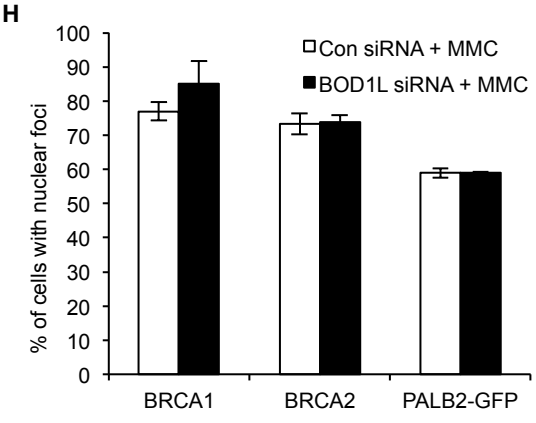
H
Con siRNA + MMC
BOD1L siRNA + MMC
% of cells with nuclear foci
BRCA1
BRCA2
PALB2-GFP

Figure 7

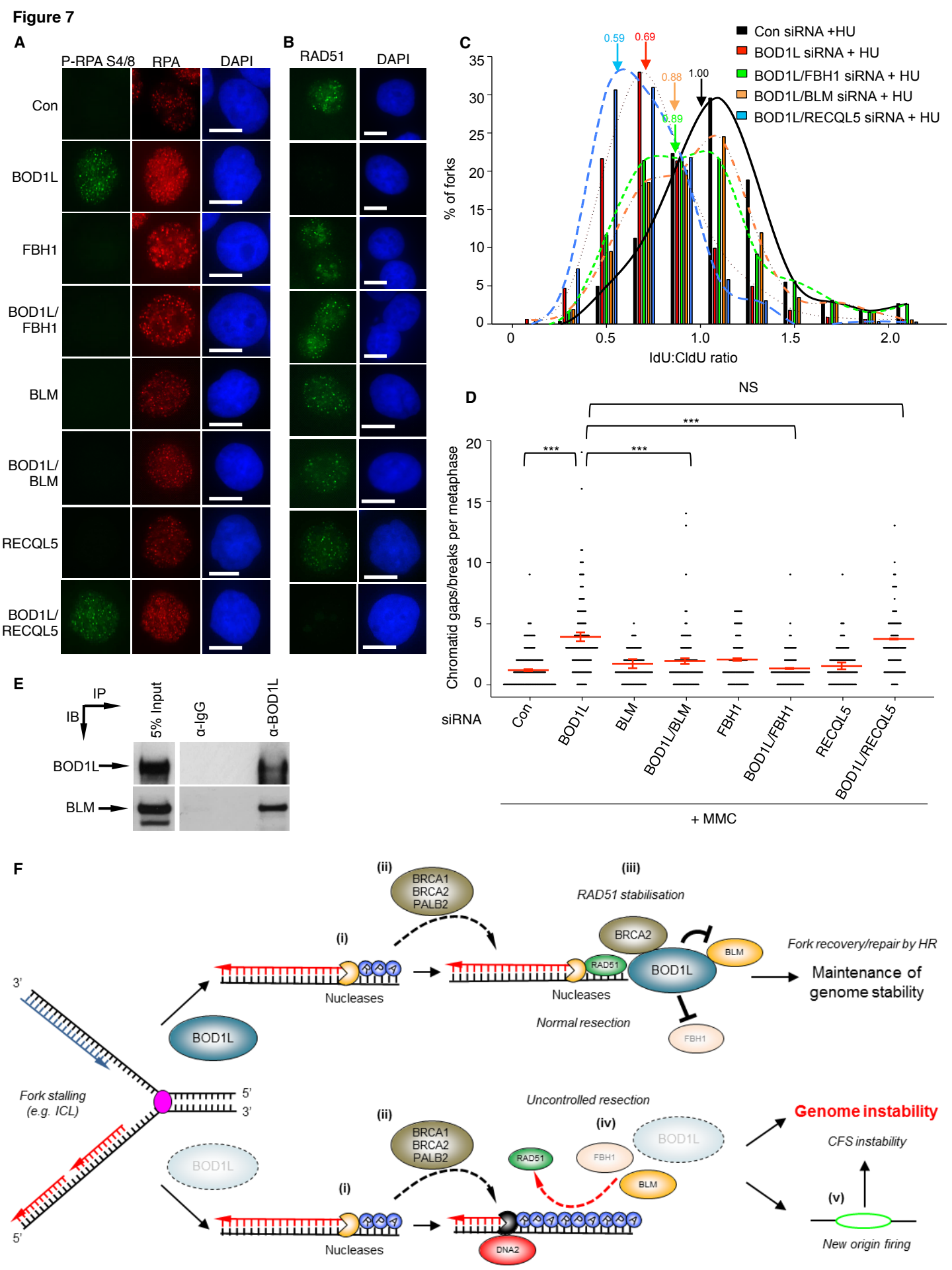
A
P-RPA S4/8
RPA
DAPI
Con
BOD1L
FBH1
BOD1L/ FBH1
BLM
BOD1L/ BLM
RECQL5
BOD1L/ RECQL5
B
RAD51
DAPI
C
Con siRNA +HU
BOD1L siRNA + HU
BOD1L/FBH1 siRNA + HU
BOD1L/BLM siRNA + HU
BOD1L/RECQL5 siRNA + HU
0.59
0.69
0.88
1.00
0.89
% of forks
IdU:CldU ratio
D
NS
***
***
***
Chromatid gaps/breaks per metaphase
siRNA
Con
BOD1L
BLM
BOD1L/BLM
FBH1
BOD1L/FBH1
RECQL5
BOD1L/RECQL5
+ MMC
E
IP
IB
5% Input
α-IgG
α-BOD1L
BOD1L
BLM
F
(i)
(ii)
(iii)
(iv)
(v)
BRCA1
BRCA2
PALB2
RAD51 stabilisation
Nucleases
BOD1L
BRCA2
RAD51
BLM
FBH1
Fork recovery/repair by HR
Maintenance of genome stability
Normal resection
Fork stalling (e.g. ICL)
3'
5'
Uncontrolled resection
DNA2
Genome instability
CFS instability
New origin firing

Figure S1

A

Protein ID	No. of peptides
PCNA	**9**
Pol δ p66 subunit	3
Pol δ p50 subunit	7
Pol δ cat. subunit	20
Pol α B subunit	3
Pol α cat. subunit	9
RFC1	5
RFC2	5
RFC3	6
RFC4	10
RFC5	7
MCM2	21
MCM3	22
MCM4	26
MCM5	17
MCM6	17
MCM7	23
RPA1	**16**
RPA2	3
RPA3	**1**
PSF3	1
BOD1L	6

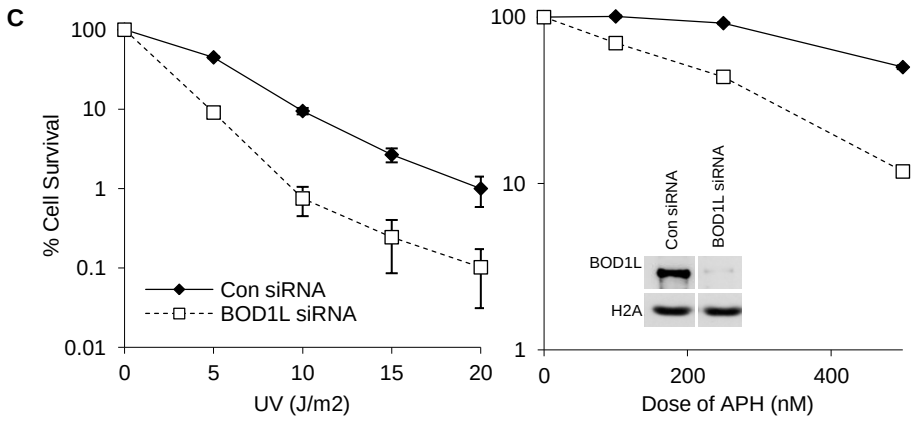

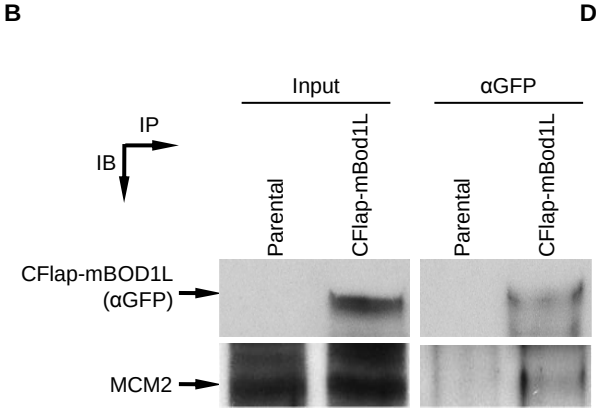

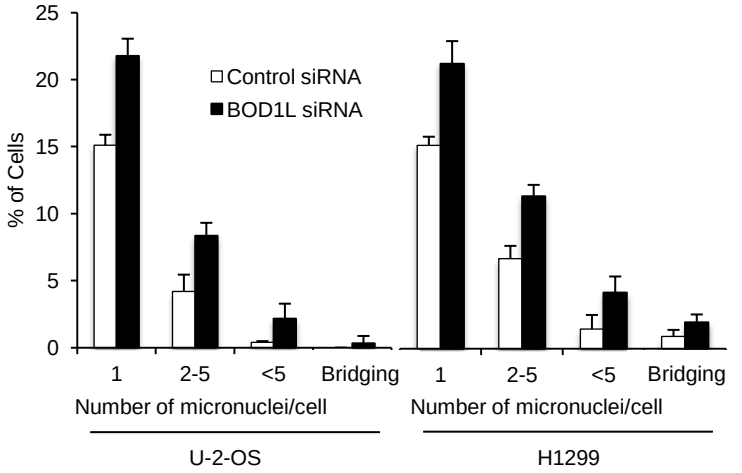

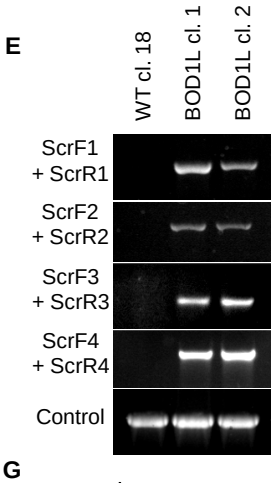

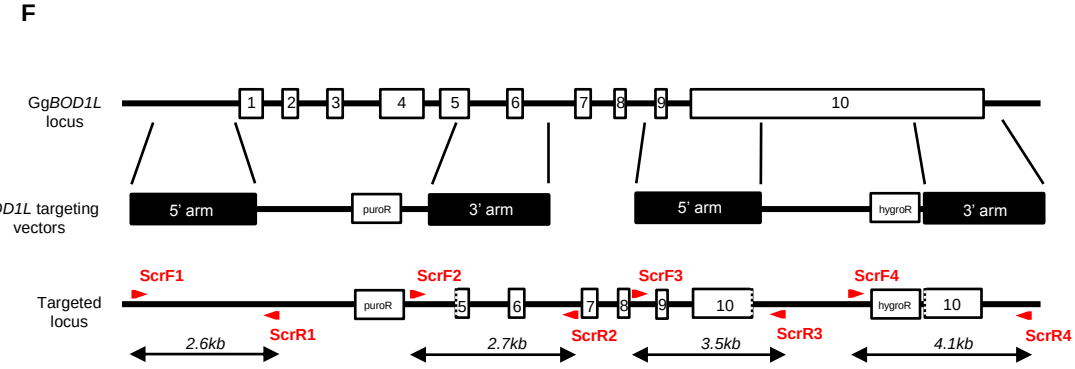

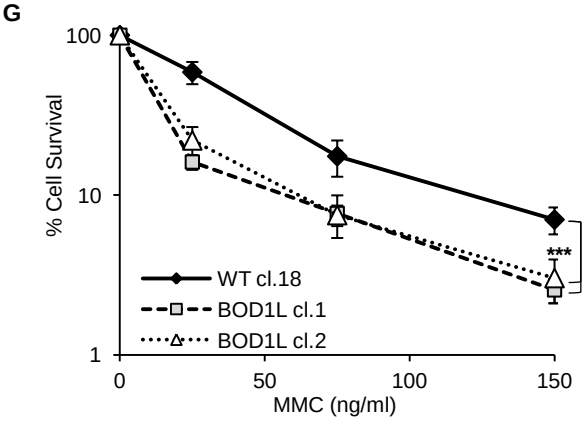

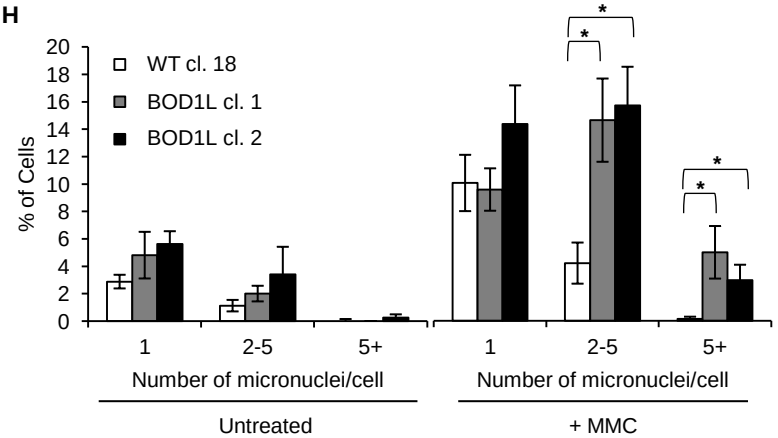

Figure S2

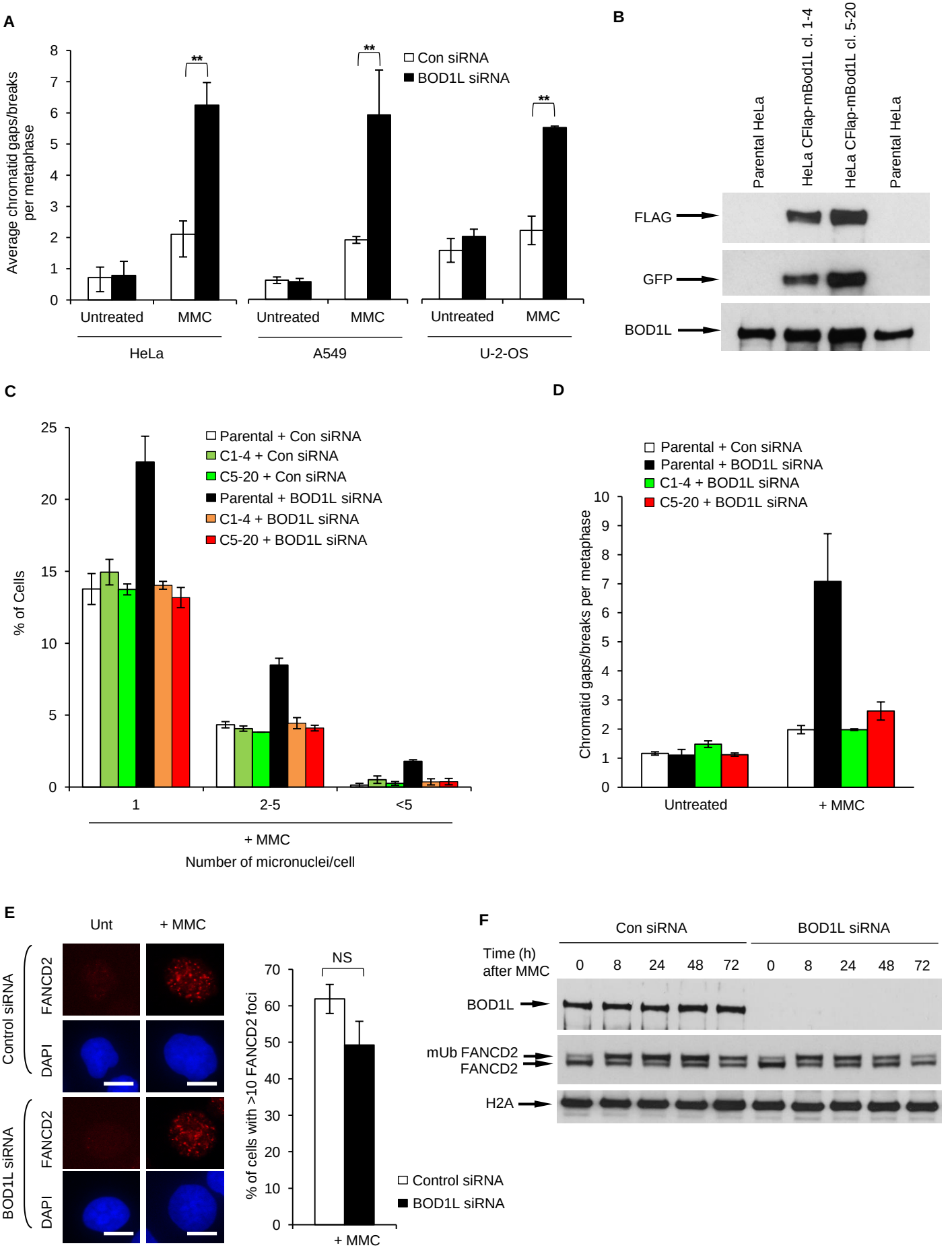
A
Average chromatid gaps/breaks per metaphase
Con siRNA
BOD1L siRNA
**
Untreated
MMC
HeLa
A549
U-2-OS
B
Parental HeLa
HeLa CFlap-mBod1L cl. 1-4
HeLa CFlap-mBod1L cl. 5-20
Parental HeLa
FLAG
GFP
BOD1L
C
% of Cells
Parental + Con siRNA
C1-4 + Con siRNA
C5-20 + Con siRNA
Parental + BOD1L siRNA
C1-4 + BOD1L siRNA
C5-20 + BOD1L siRNA
1
2-5
<5
+ MMC
Number of micronuclei/cell
D
Chromatid gaps/breaks per metaphase
Parental + Con siRNA
Parental + BOD1L siRNA
C1-4 + BOD1L siRNA
C5-20 + BOD1L siRNA
Untreated
+ MMC
E
Unt
+ MMC
Control siRNA
BOD1L siRNA
FANCD2
DAPI
NS
% of cells with >10 FANCD2 foci
Control siRNA
BOD1L siRNA
+ MMC
F
Con siRNA
BOD1L siRNA
Time (h) after MMC
0 8 24 48 72 0 8 24 48 72
BOD1L
mUb FANCD2
FANCD2
H2A

Figure S3

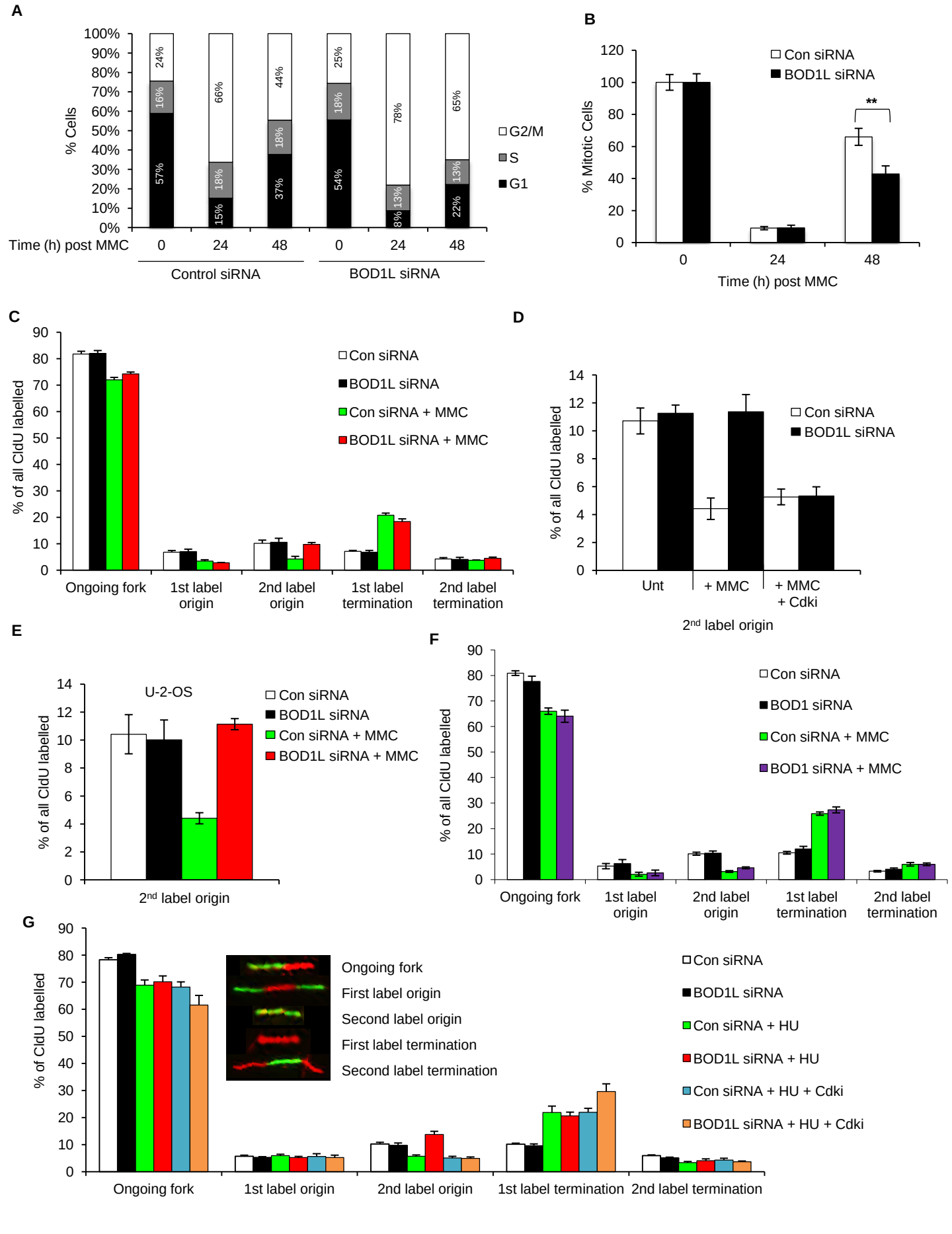
A
100%
90%
80%
70%
60%
50%
40%
30%
20%
10%
0%
% Cells
24%
16%
57%
66%
18%
15%
44%
18%
37%
25%
18%
54%
78%
13%
8%
65%
13%
22%
G2/M
S
G1
Time (h) post MMC
0
24
48
0
24
48
Control siRNA
BOD1L siRNA
B
120
100
80
60
40
20
0
% Mitotic Cells
Con siRNA
BOD1L siRNA
**
0
24
48
Time (h) post MMC
C
90
80
70
60
50
40
30
20
10
0
% of all CldU labelled
Con siRNA
BOD1L siRNA
Con siRNA + MMC
BOD1L siRNA + MMC
Ongoing fork
1st label origin
2nd label origin
1st label termination
2nd label termination
D
14
12
10
8
6
4
2
0
% of all CldU labelled
Con siRNA
BOD1L siRNA
Unt
+ MMC
+ MMC + Cdki
2nd label origin
E
U-2-OS
14
12
10
8
6
4
2
0
% of all CldU labelled
Con siRNA
BOD1L siRNA
Con siRNA + MMC
BOD1L siRNA + MMC
2nd label origin
F
90
80
70
60
50
40
30
20
10
0
% of all CldU labelled
Con siRNA
BOD1 siRNA
Con siRNA + MMC
BOD1 siRNA + MMC
Ongoing fork
1st label origin
2nd label origin
1st label termination
2nd label termination
G
90
80
70
60
50
40
30
20
10
0
% of CldU labelled
Ongoing fork
First label origin
Second label origin
First label termination
Second label termination
Con siRNA
BOD1L siRNA
Con siRNA + HU
BOD1L siRNA + HU
Con siRNA + HU + Cdki
BOD1L siRNA + HU + Cdki
Ongoing fork
1st label origin
2nd label origin
1st label termination
2nd label termination

Figure S4

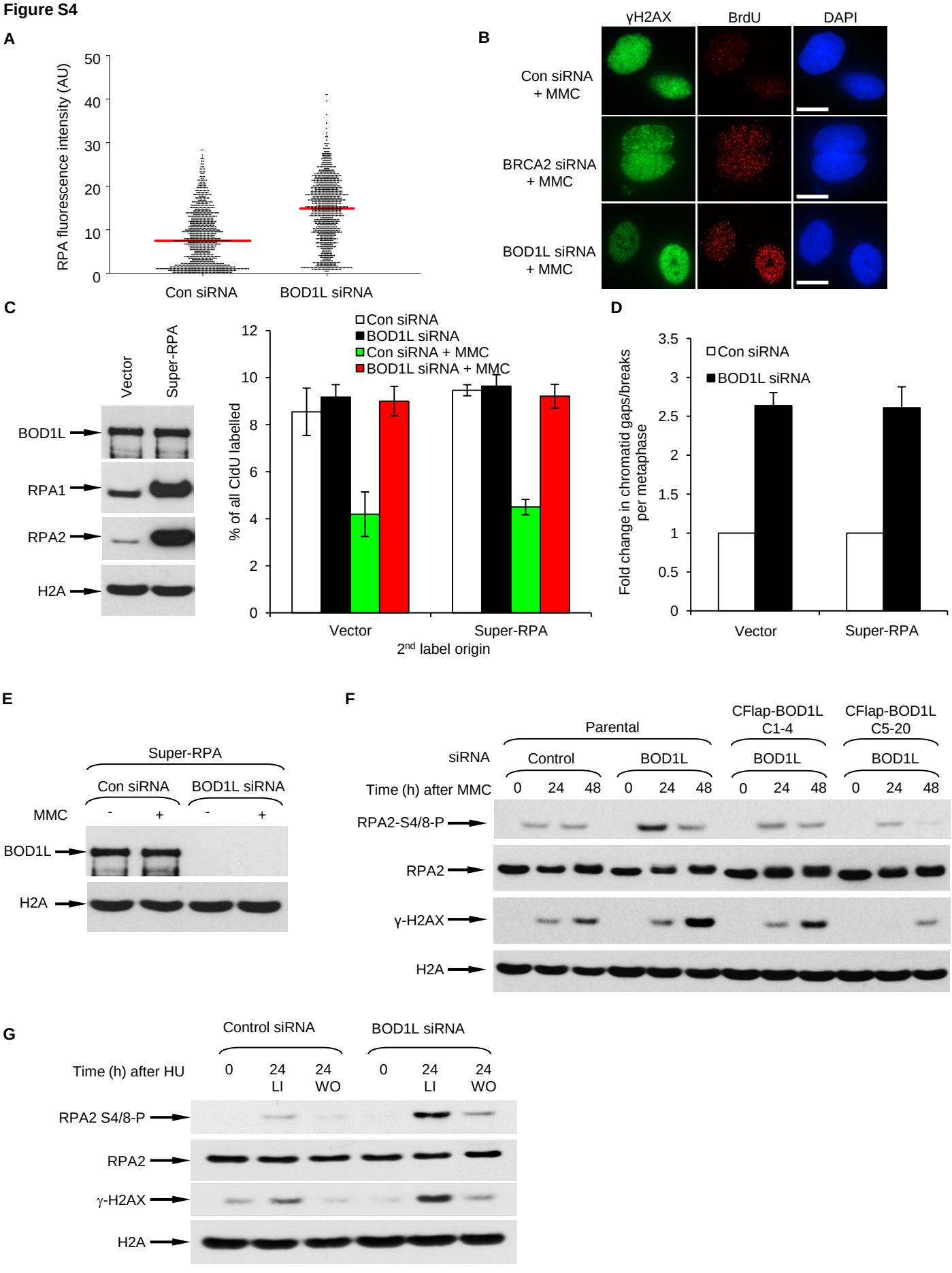
A
RPA fluorescence intensity (AU)
50
40
30
20
10
0
Con siRNA
BOD1L siRNA
B
γH2AX
BrdU
DAPI
Con siRNA + MMC
BRCA2 siRNA + MMC
BOD1L siRNA + MMC
C
Vector
Super-RPA
BOD1L
RPA1
RPA2
H2A
Con siRNA
BOD1L siRNA
Con siRNA + MMC
BOD1L siRNA + MMC
% of all CldU labelled
12
10
8
6
4
2
0
Vector
Super-RPA
2nd label origin
D
Con siRNA
BOD1L siRNA
Fold change in chromatid gaps/breaks per metaphase
3.5
3
2.5
2
1.5
1
0.5
0
Vector
Super-RPA
E
Super-RPA
Con siRNA
BOD1L siRNA
MMC
-
+
-
+
BOD1L
H2A
F
Parental
CFlap-BOD1L C1-4
CFlap-BOD1L C5-20
siRNA
Control
BOD1L
BOD1L
BOD1L
Time (h) after MMC
0
24
48
0
24
48
0
24
48
0
24
48
RPA2-S4/8-P
RPA2
γ-H2AX
H2A
G
Control siRNA
BOD1L siRNA
Time (h) after HU
0
24 LI
24 WO
0
24 LI
24 WO
RPA2 S4/8-P
RPA2
γ-H2AX
H2A

Figure S5

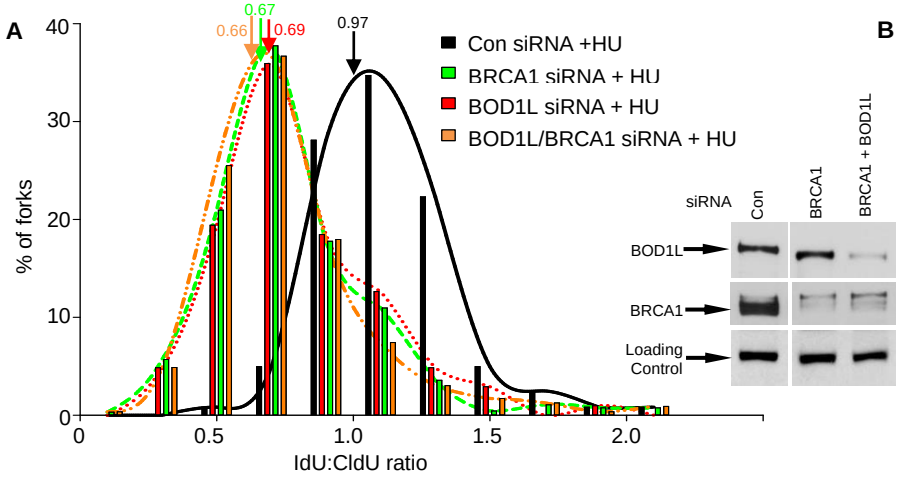

B

	Average IdU:CldU ratio	SEM
Con siRNA	1.02	0.01
BRCA1 siRNA	1.02	0.01
BRCA2 siRNA	1.02	0.03
BOD1L siRNA	1.00	0.02
BOD1L/BRCA1 siRNA	0.99	0.03
BOD1L/BRCA2 siRNA	1.01	0.01
Con siRNA + HU	0.97	0.03
BRCA1 siRNA + HU	0.67	0.04
BRCA2 siRNA + HU	0.69	0.02
BOD1L siRNA + HU	0.68	0.03
BOD1L/BRCA1 siRNA + HU	0.66	0.03
BOD1L/BRCA2 siRNA + HU	0.64	0.02

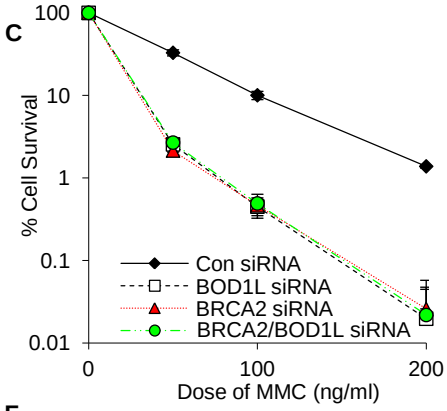

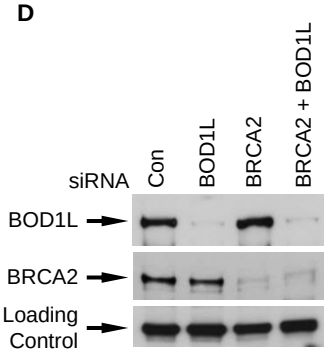

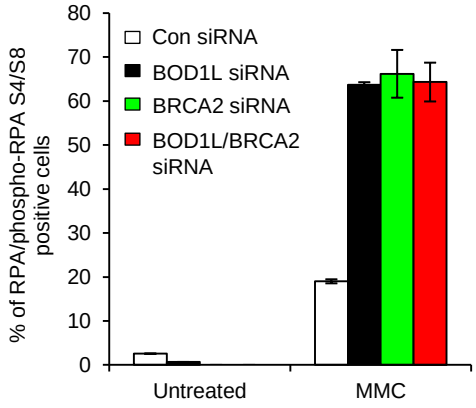

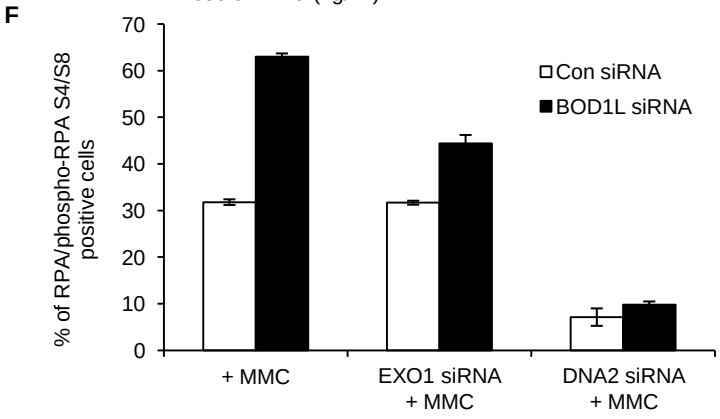

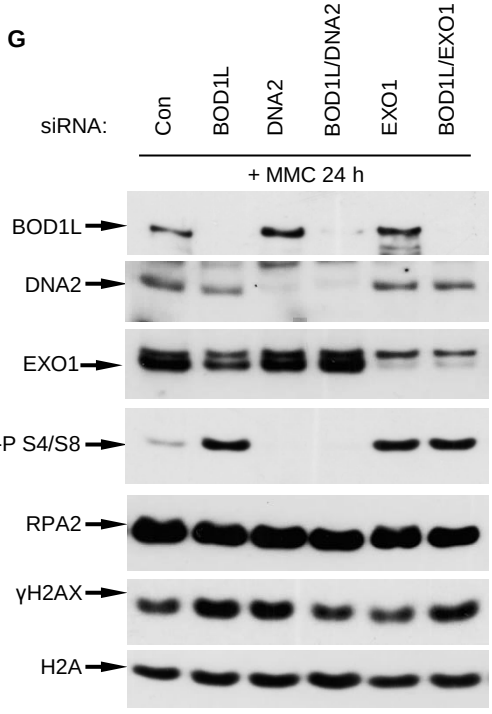

H

	Untreated		+ HU	
	Average IdU:CldU ratio	SEM	Average IdU:CldU ratio	SEM
Con siRNA	1.01	0.03	1.03	0.01
BOD1L siRNA	1.02	0.01	0.70	0.02
BOD1L/DNA2 siRNA	1.02	0.04	0.99	0.01
BOD1L siRNA + Mirin	ND	ND	0.68	0.01

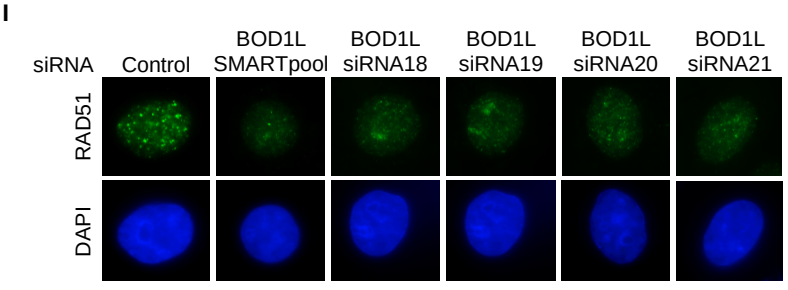

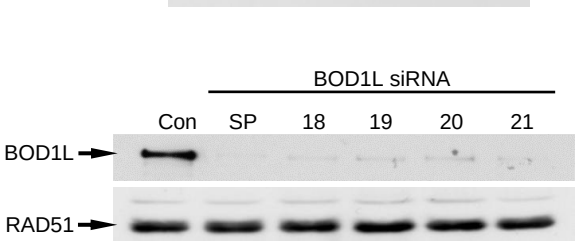

Figure S6

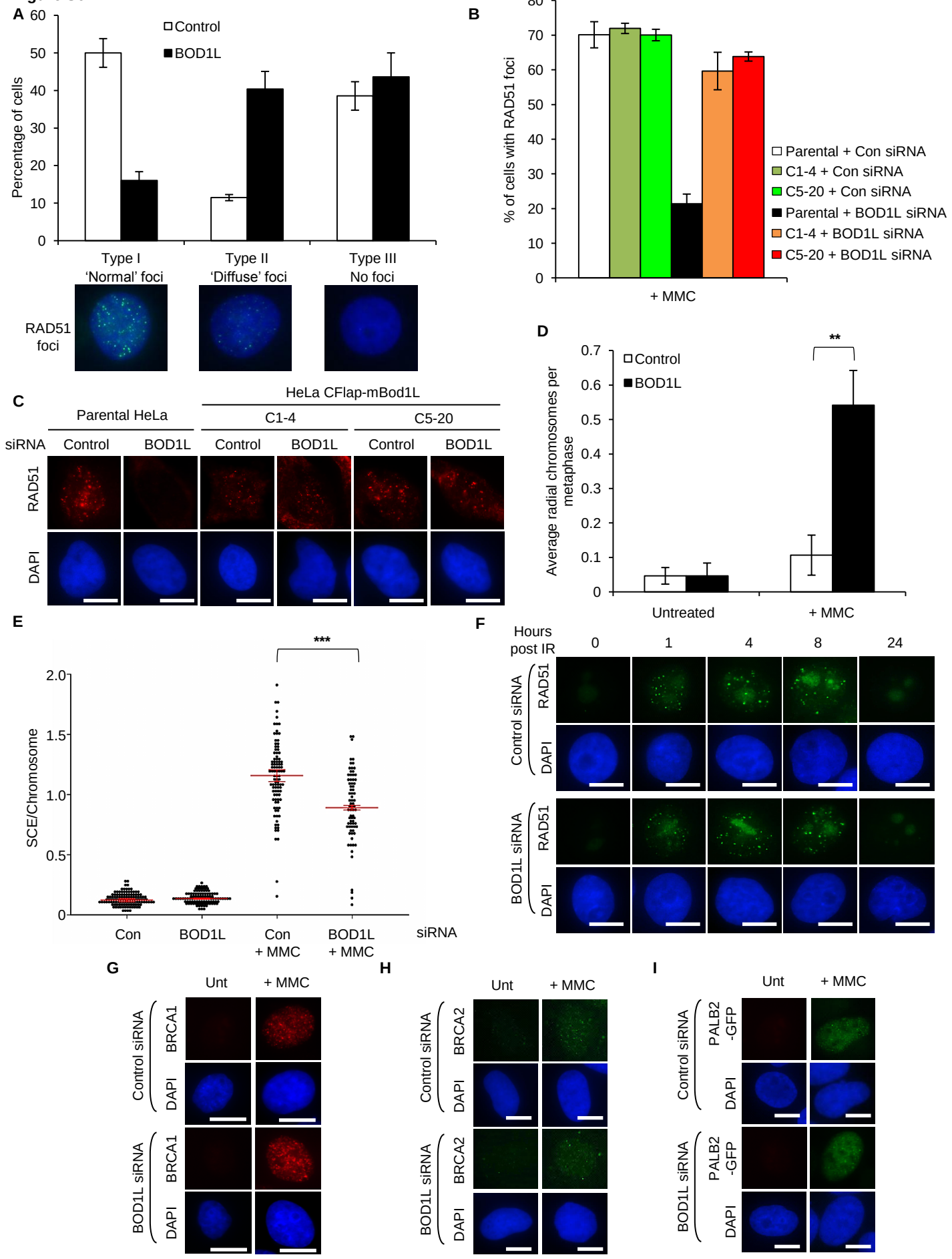
A
Control
BOD1L
Percentage of cells
Type I
'Normal' foci
Type II
'Diffuse' foci
Type III
No foci
RAD51
foci
B
% of cells with RAD51 foci
Parental + Con siRNA
C1-4 + Con siRNA
C5-20 + Con siRNA
Parental + BOD1L siRNA
C1-4 + BOD1L siRNA
C5-20 + BOD1L siRNA
+ MMC
C
HeLa CFlap-mBod1L
Parental HeLa
C1-4
C5-20
siRNA
Control
BOD1L
RAD51
DAPI
D
Control
BOD1L
Average radial chromosomes per metaphase
**
Untreated
+ MMC
E
***
SCE/Chromosome
Con
BOD1L
Con + MMC
BOD1L + MMC
siRNA
F
Hours post IR
0
1
4
8
24
Control siRNA
BOD1L siRNA
RAD51
DAPI
G
Unt
+ MMC
Control siRNA
BOD1L siRNA
BRCA1
DAPI
H
Unt
+ MMC
Control siRNA
BOD1L siRNA
BRCA2
DAPI
I
Unt
+ MMC
Control siRNA
BOD1L siRNA
PALB2 -GFP
DAPI

Figure S7

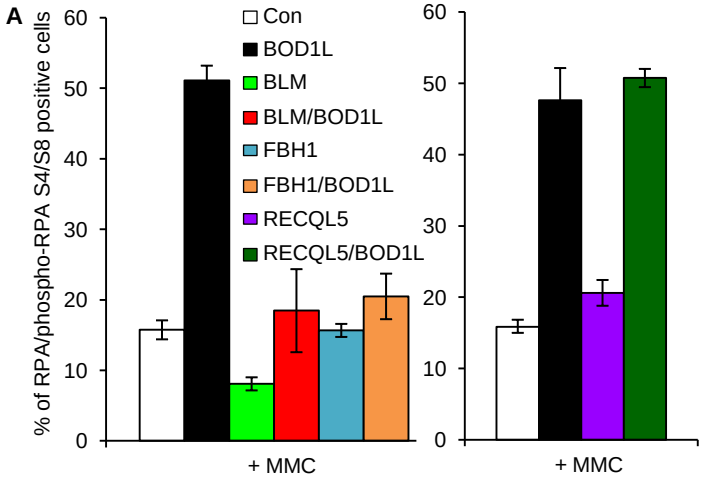

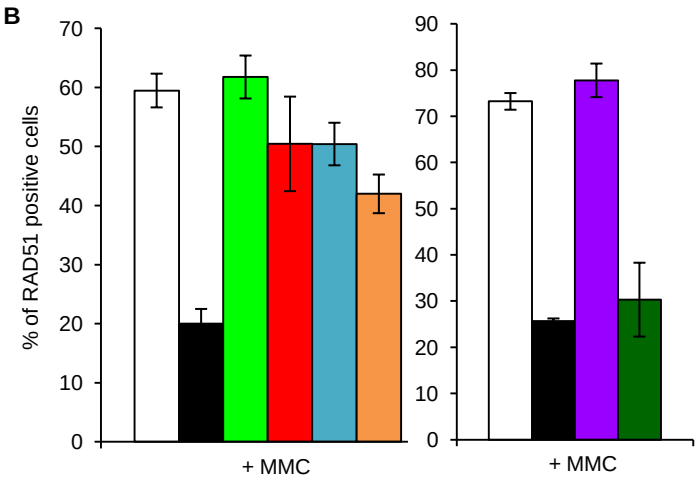

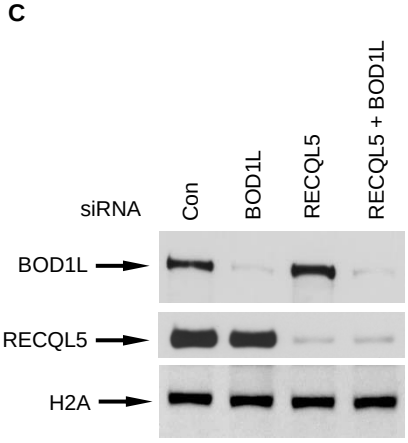

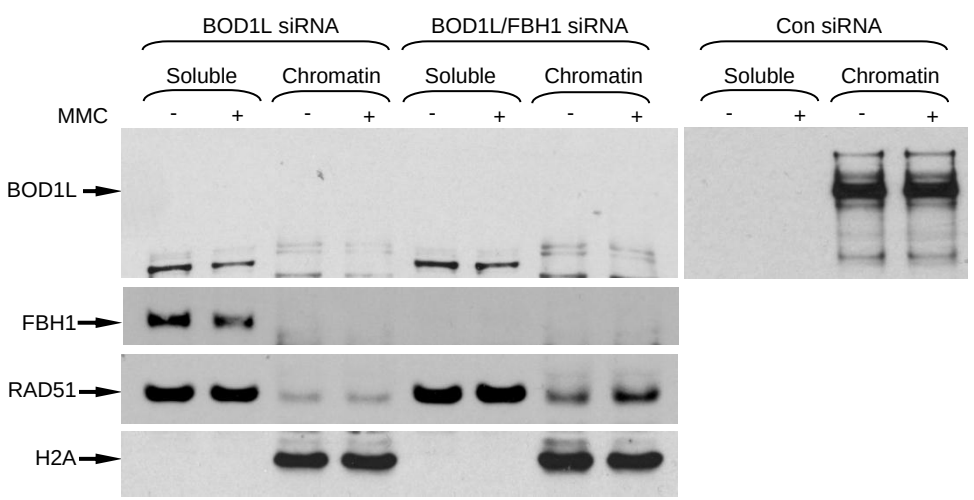

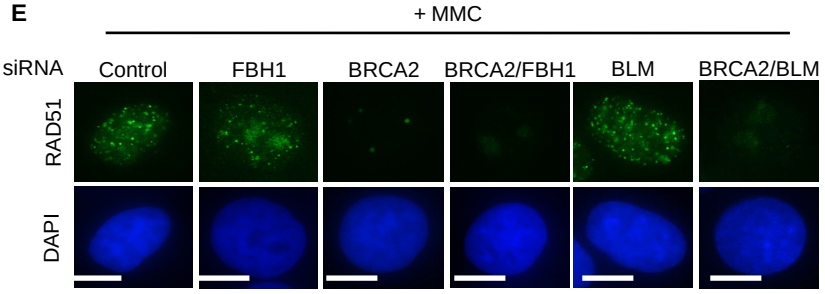

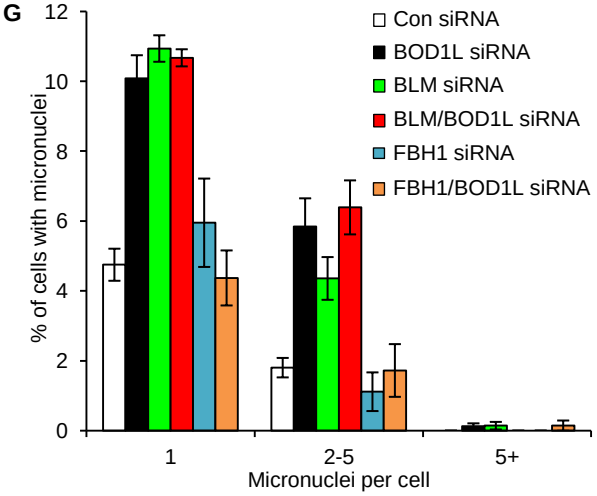

F

	Untreated		+ HU	
	Average IdU:CldU ratio	SEM	Average IdU:CldU ratio	SEM
Con siRNA	1.02	0.01	1.00	0.01
BOD1L siRNA	1.02	0.02	0.69	0.02
FBH1 siRNA	ND	ND	ND	ND
BOD1L/FBH1 siRNA	0.99	0.02	0.90	0.03
BLM siRNA	ND	ND	ND	ND
BOD1L/BLM siRNA	0.97	0.01	0.88	0.01
RECQL5 siRNA	1.00	0.03	0.75	0.05
BOD1L/RECQL5 siRNA	0.99	0.01	0.59	0.01

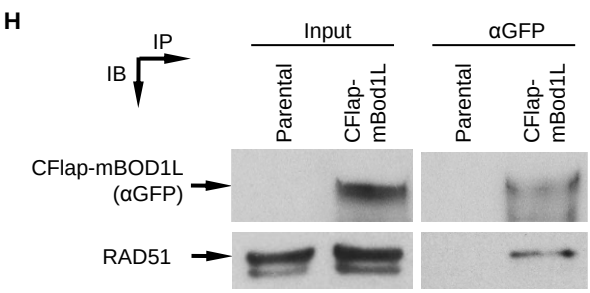

SUPPLEMENTAL FIGURE LEGENDS

Figure S1: BOD1L ensures cellular viability and genome integrity after replication stress. Related to Figure 1. (A) Total peptides identified by mass spectroscopy analysis of EdU-coprecipitates isolated from HeLa S3 cells. A complete mass spectrometry data set is available on request to the Corresponding Author. **(B)** WCE from parental HeLa or HeLa-CFlap-mBod1L cells (clone 5-20; see also **Figure S2B**) were subjected to IP with anti-GFP antibody, and inputs and recovered immunoprecipitates were analyzed by immunoblotting. Blots originate from a single gel. A white line denotes removal of irrelevant lanes. **(C)** HeLa cells were transfected with the indicated siRNA for 72 h and exposed to the indicated doses of UV-C or aphidicolin (APH), left to form colonies for 14 days, and then stained with methylene blue and counted. **(D)** U-2-OS and H1299 cells were transfected as in (C), exposed to 50 ng/ml MMC for 24 h, and micronuclei formation was assessed by immunofluorescence. **(E)** PCR screening of WT and BOD1L-deleted (Δexon 1/Δexon 10) DT40 clones using the primers in (F). The presence of PCR products denotes successful recombination of the homology arms, and thus deletion of the desired region. **(F)** Schematic of the *Gallus gallus* BOD1L locus (*upper*) with targeting vectors spanning exons 1-5 and exon 10 (*middle*), and a schematic of the targeted Δexon 1/Δexon 10 locus (*lower*). Positions of screening primers are shown. **(G)** WT DT40s, and two clones lacking exons 1-5 and exon 10 of BOD1L, were exposed to the indicated doses of MMC, left to form colonies in soft agar, stained with methylene blue and counted. Plots represent mean data from four independent experiments; error bars represent SEM. Two-way ANOVA. **(H)** WT or BOD1L-deleted DT40s were exposed to 12.5 ng/ml MMC for 24 h, and micronuclei formation assessed by immunofluorescence. Plots represent mean data from three independent experiments; error bars represent SEM; Student's t-test. * = $p<0.05$; *** = $p<0.001$.

Figure S2: BOD1L knockdown increases genomic instability after replication stress. Related to Figure 3. (A) HeLa, A549 and U-2-OS cells were treated as in **Figure 3G**, and damage to metaphase chromosomes was analysed by Geimsa staining and light microscopy.

Graphs integrate data from 50 cells for each condition from three independent experiments. **(B-D)** Parental HeLa or HeLa-CFlap-mBod1L cells (clones C1-4 and C5-20) were transfected with the indicated siRNA for 72 h, and: (B) Whole cell extracts of cells (WCE) were analysed by immunoblotting; (C) Micronuclei formation was assessed by immunofluorescence; (D) Metaphase chromosomes were analysed by Geimsa staining and light microscopy. **(E)** HeLa cells from **Figure 3A** were immunostained with antibodies to FANCD2, and foci formation analysed by fluorescence microscopy. Plot indicates quantification of cells with more than 10 FANCD2 foci per cell from four independent experiments. **(F)** U-2-OS cells were transfected with the indicated siRNA for 72 h, exposed to 250 ng/ml MMC for 3 h, left to recover for the indicated times, and WCE were analysed by immunoblotting. Scale bars = 10 μm. NS = $p>0.05$; ** = $p<0.01$; Students' t-test.

Figure S3: The effect of BOD1L depletion on DNA replication kinetics. Related to Figure 4. **(A)** Quantification of cell cycle profiles shown in **Figure 4B**. Data is representative of the mean ± SEM of four independent experiments. **(B)** Cells from (A) were immunostained with antibodies to phosphorylated histone H3-Ser10, and the percentage of mitotic cells determined by flow cytometry. Data represent mean ± SEM of four independent experiments. **(C)** DNA fibres from **Figure 4E** were quantified. The percentages of ongoing forks, first-label (bidirectional) origins, new origins (IdU-labelled only), first-label terminations (CldU-labelled only) and second label terminations are displayed. **(D)** HeLa cells were treated as in **Figure 4E** except that, where indicated, they were treated with CDK1/2 inhibitor for 3 h prior to pulse labelling. Plot displays percentage of new origins (IdU-labelled only). **(E)** U-2-OS cells were transfected with the indicated siRNA for 72 h, and DNA fibres prepared as in **Figure 4E**. The percentage of new origins (IdU-labelled only) is displayed. **(F)** HeLa cells were transfected with the indicated siRNAs, and the DNA combed and analysed as above. **(G)** Cells were treated as in **Figure 4D**, except that, where indicated, they were treated with CDK1/2 inhibitor for the duration of HU exposure (2 h). Plots display average percentages of the relevant fork

structure(s) from three independent experiments; error bars represent SEM. ** = p<0.01; Students' t-test.

Figure S4: BOD1L is necessary to prevent excessive ssDNA formation and RPA2 hyper-phosphorylation after replication stress. Related to Figure 5. **(A)** Foci formation in HeLa cells from **Figure 5B** was analysed by fluorescence microscopy, and fluorescence intensity per nucleus was quantified using ImageJ. Lines denote mean values from three independent experiments. **(B)** U-2-OS cells were treated as in **Figure 5C**, and immunostained with antibodies to BrdU and γH2AX. Representative images are shown. Scale bars = 10 μm. **(C-E)** Vector U-2-OS or SUPER-RPA U-2-OS cells were transfected with the indicated siRNAs and exposed to 50 ng/ml MMC for 24 h. (C) *Left panel*: WCE of the indicated cell lines were analysed by immunoblotting. *Right panel*: Transfected Vector or SUPER-RPA cells were treated as in **Figure 4E**, and the plots display the percentage of new origins (IdU-labelled only). (D) Damage to metaphase chromosomes was analysed by Geimsa staining and light microscopy. Graphs integrate data from 150 cells, in total, for each condition from three independent experiments, and are displayed as fold change compared to control siRNA-transfected cells. (E) WCE of the indicated cell lines were analysed by immunoblotting. **(F)** Parental HeLa or HeLa-CFlap-mBod1L cells (clones C1-4 and C5-20) were transfected with the indicated siRNA for 72 h, exposed to 50 ng/ml MMC for 24 or 48 h, and WCE were analysed by immunoblotting. **(G)** HeLa cells were transfected with the indicated siRNA for 72 h, exposed to 250 μM HU for 24 h, and harvested immediately (LI), or left to recover for a further 24 h (WO). WCE were analysed by immunoblotting.

Figure S5: BOD1L is required to suppress aberrant end resection at replication forks after replication stress. Related to Figure 6. **(A)** U-2-OS cells were transfected with the indicated siRNAs for 72 h, pulsed for 20 min each with CldU and IdU, and exposed to 4 mM HU for 5 h. DNA was visualised with antibodies to CldU and IdU, and replication fork length was calculated. Plots denote the average ratios of IdU:CldU label lengths from three

independent experiments. Arrows indicate mean ratios. (*Inset*) WCE of cells were analysed by immunoblotting. Control siRNA panel is from the same gel as in **Figure S7C**. A white line denotes removal of irrelevant lanes. **(B)** Average values of IdU:CldU label lengths from DNA isolated from cells in **Figures 6A and S6A** is indicated, and SEM are denoted. **(C)** HeLa cells were transfected for 72 h with the indicated siRNAs, exposed to the indicated doses of MMC, left to form colonies for 14 days, and then stained with methylene blue and counted. Plots denote the average values from three independent experiments. **(D)** WCE of cells from (C) were analysed by immunoblotting. Loading control denotes a non-specific protein detected by anti-BOD1L antibody. **(E)** HeLa cells from (C) were exposed to 50 ng/ml MMC for 24 h, immunostained with antibodies to RPA2 and phospho-RPA S4/S8, and foci formation was analysed by fluorescence microscopy. The average percentage of double-positive cells is shown. **(F)** HeLa cells were transfected with the indicated siRNA for 72 h, exposed to 50 ng/ml MMC for 24 h, immunostained with antibodies to RPA2 and phospho-RPA S4/S8, and foci formation was analysed by fluorescence microscopy. The average percentage of double-positive cells from three independent experiments is shown. **(G)** WCE of HeLa cells from (F) were analysed by immunoblotting. **(H)** DNA from U-2-OS cells in **Figure 6C** was visualised with antibodies to CldU and IdU, and replication fork length was calculated. Average values and SEM are denoted. **(I-J)** HeLa cells were transfected with the indicated siRNAs, exposed to 50 ng/ml MMC for 24 h, and either: RAD51 foci formation was analysed by fluorescence microscopy (I); or RAD51 expression was analysed by immunoblotting (J). siRNAs18-21 were individual siRNAs from the SMARTpool.

Figure S6: BOD1L enables RAD51 chromatin loading to promote efficient homologous recombination. Related to Figure 6. (A) HeLa cells were transfected with the indicated siRNA for 72 h, exposed to 50 ng/ml MMC for 24 h, and immunostained with antibodies to RAD51. Foci formation was analysed by fluorescence microscopy, and quantified into three distinct phenotypes (representative images are shown in the lower panel). **(B-C)** Parental HeLa or HeLa-CFlap-mBod1L cells (clones C1-4 and C5-20) were transfected with the

indicated siRNA for 72 h, exposed to 50 ng/ml MMC, and immunostained with antibodies to RAD51. (B) Foci formation was analysed by fluorescence microscopy and quantified. (C) Representative images are shown. **(D)** The incidence of radial chromosome formation was analysed from metaphase spreads prepared as described in **Figure 3G**. ** = p<0.01; Students' t-test. **(E)** HeLa cells were transfected with the indicated siRNA for 24 h, labelled with BrdU for a further 24 h, and exposed to 25 ng/ml MMC for a further 24 h. Sister chromatid exchanges were quantified from at least 50 cells from three independent metaphase spreads. Line = mean number of SCEs/chromosome. Error bars = SEM. *** = p<0.001; Mann-Whitney ranked sum test. **(F)** HeLa cells were transfected with the indicated siRNA for 72 h, exposed to 5 Gy of γ-irradiation, and immunostained with antibodies to RAD51. Scale bars = 10 μm. **(G-I)** The prevalence of nuclear foci of BRCA1, BRCA2, and PALB2-GFP in HeLa or U-2-OS-PALB2-GFP cells from **Figure 6H**. Foci formation was analysed by fluorescence microscopy, and representative images are shown.

Figure S7: BOD1L acts to restrain anti-recombinase activity to stabilise RAD51 chromatin loading and prevent excessive resection of replication forks. Related to Figure 7. (A-B) HeLa cells were treated as in **Figure 7A/B**, and RPA2/RPA2-PS4/8 foci formation (A) or RAD51 foci formation (B) was analysed by fluorescence microscopy. The average percentage of double-positive cells (A) or RAD51-positive cells (B) is shown. **(C)** WCE of cells from (A) were analysed by immunoblotting. **(D)** U-2-OS cells were transfected with the indicated siRNAs, exposed to 100 ng/ml MMC for 24 h, and then fractionated. Soluble and chromatin fractions were analysed by immunoblotting. Blots originate from a single gel. A white line denotes removal of irrelevant lanes. **(E)** HeLa cells were transfected with the indicated siRNA for 72 h, exposed to 50 ng/ml MMC for 24h, and immunostained with antibodies to RAD51. Scale bars = 10 μm. **(F)** U-2-OS cells were treated as in **Figure 7C**, and IdU:CldU ratios were calculated in the presence/absence of HU. Average values and SEM are denoted. **(G)** Micronuclei formation was assessed by immunofluorescence in HeLa cells from **Figure 7A**. **(H)** WCE from parental HeLa or HeLa-CFlap-mBod1L cells from **Figure S1B** were

subjected to IP with anti-GFP antibody, and inputs and recovered immunoprecipitates were analyzed by immunoblotting. The upper panel is identical to that shown in **Figure S1B**. A white line denotes removal of irrelevant lanes.

SUPPLEMENTAL EXPERIMENTAL PROCEDURES

Cell lines

A549, HeLa, HeLa S3, U-2-OS, and H1299 were sourced from the ATCC. U2OS-PALB2-GFP were obtained from F. Esashi. HeLa-FUCCI were obtained from RIKEN BRC.

Drugs and inhibitors

HU, Aphidicolin, and MMC were from Sigma Aldrich, and were used as indicated in the Figure Legends. Cdk1/2 inhibitor III was used at 25 μM (Merck). dNTP analogues BrdU, EdU, CldU and IdU were from Sigma Aldrich, and were used as indicated. Mirin (Calbiochem) was used at 50 μM.

Generation of HeLa-CFlap-BOD1L cells.

A BAC containing the full length *Mus musculus* BOD1L locus was obtained from BacPac Resources. This BAC was modified to insert a C-terminal Flap tag by Red/ET recombination following a modified protocol from Genebridges. To generate HeLa-CFlap-BOD1L cells, HeLa cells have been transfected with CFlap-Bod1L BAC using Lipofectamine 2000 (Invitrogen), then selected for 3 weeks with Geneticin and single cell-sorted by FACS following high level of GFP expression. Two clones (C1-4 and C5-20) were expanded and used for further experiments.

Generation of BOD1L knock out DT40 cell lines.

BOD1L knock out DT40 cell lines were generated using two disruption cassettes targeting exons 1-5 and targeting exon 10 of the chicken BOD1L locus. The chicken BOD1L locus was identified by BLAST search using the human protein sequence against the ENSEMBL draft chicken genome sequence. An ENSEMBL predicted transcript encompassed the entire BOD1L gene. From this sequence, two disruption cassettes targeting exons 1-5 and targeting exon 10 were designed. PCR oligos used to amplify 5′ and 3′ arms of the first construct targeting exons 1-5 were

GCGGCCGCGGTCTCGGATCCATGGAGCGACAATGATGACACAGATGG/ GGTGATATCGGCGGCAAGCTGGCTACAGCGTGTTAGGAGGGTTGAGTG and ATTATACGAACGGTACTCGATGATTTGAAGAGGAAAGTGAAGAAGAACCTGTG/ GGATCCGAGACCGCGGCCGCCCTATCTTACTCACCACCCCCAAGTCCTCA respectively. PCR oligos used to amplify 5′ and 3′ arms of the second construct targeting exon 10 were AATATAAAGCTTGCGGCCGCCAGCGTTGTCCAAAGGACATCTG/ GTCAAGCTTCTATTTGGCATCTGTGGCTTGGACTG and GTACTTGAGTAGCGTGTAATCAGTGCAAGTGCTGATG/ GGCAAGCTTATAGCAGGGTGGGTTGGAACTAGATG respectively. Targeting constructs were generated by cloning the PCR products into the pSH vector containing either puromycin or hygromycin resistance. Transfections and selection of targeted DT40 clones were carried out as described previously (Niedzwiedz *et al*., 2004). To confirm the appropriate disruptions of the GgBOD1L locus, genomic DNA was obtained and the following PCR oligos were used to screen the clones: ScrF1, TGCATCAGGGATGCACATTCTC; ScrR1, TAAGACTGCTGCTGACACCTTCAC; ScrF2, GCGGGACTATGGTTGCTGACTAATTGAG; ScrR2, ACTAGCTGCGTCCCAAAGAGTTTC; ScrF3, GCTGGCATGCTGGAATGTACTTTATGG; ScrR3, CTTCACAGAGGCGAGTAACTTCCTGTAAC; ScrF4, ACGATTCCGAAGCCCAACCTTTCATAG; ScrR4, ATCTTTGGAGATGTTCAAGGCCAGGTC (**Figure S1E**).

siRNA Transfections

siRNAs were from Dharmacon as SMARTpool (SP) or individual siRNAs deconvolved from the SMARTpool: BOD1L (SP, siRNA-18,-19,-20,-21); BOD1 (SP). SP and BOD1L siRNA-19 were used for all experiments unless stated. siRNA transfections were performed with siRNA duplexes (100 nM) using Oligofectamine (Invitrogen). Whenever siRNAs were combined, the total concentration was kept at 100 nM. A custom siRNA targeting lacZ (CGUACGCGGAAUACUUCGAdTdT) was used as a scrambled, non-targeting siRNA, and is

abbreviated as “Control siRNA”, or “Con siRNA”. All experiments were performed 72 h post knockdown unless otherwise stated.

Colony survival assays

Colony survival assays using HeLa cells were carried out as described (Stewart *et al.*, 2003). For colony survival assays with DT40 cells, MMC-treated cells were plated in methylcellulose after exposure to a range of concentrations of the drug. Viable colonies were scored after 2-3 weeks.

DNA combing

DNA combing was carried out essentially as described previously (Petermann *et al.*, 2010). HU (2 mM) or MMC (50 ng/ml) treatments were for 2 h or 24 h respectively. For resection experiments, cells were pulse-labelled with CldU and IdU for 20 min each before a 5 h exposure to 4 mM HU. For quantification of replication structures, at least 250 structures were counted per experiment. The lengths of red or green labelled tracts were measured using ImageJ (National Institutes of Health; http://rsbweb.nih.gov/ij/) and arbitrary length values were converted into micrometers using the scale bars created by the microscope.

Chromatin fractionation

Subcellular fractionations were performed in U-2-OS cells essentially as described in (Mendez and Stillman, 2000), except that chromatin fractions were washed once after isolation in 200 mM NaCl, 3 mM EDTA, 0.2 mM EGTA, 1 mM DTT, plus protease inhibitor cocktail, and re-suspended in UTB.

Metaphase spreads, SCEs and FISH

Chromosomal aberrations and sister chromatid exchanges (SCEs) were scored in Giemsa stained metaphase spreads. For chromosome aberrations, demecolcine (Sigma) was added 3-4 h prior to harvesting at a final concentration of 0.2 μg/ml. Cells were harvested by

trypsinisation, subjected to hypotonic shock for 1 hour at 37°C in 0.3 M sodium citrate and fixed in 3:1 methanol:acetic acid solution. Cells were dropped onto acetic acid humidified slides, stained for 15 minutes in Giemsa-modified (Sigma) solution (5% v/v in H2O) and washed in water for 5 minutes.

For SCEs, 10 μM BrdU (Sigma) was added to the medium for two complete cycles (approximately 48 hours) before collection and 25ng/ml MMC was added 24 h before collection. 0.2 μg/ml demecolcine was added 3 h prior to harvesting and metaphase spreads were obtained as described above. Before Giemsa staining, slides were incubated in Hoescht 33258 solution (10 μg/ml) for 20 minutes, exposed to UV light (355 nm) for 1 hour and washed for 1 hour at 60°C in 20× SCC. Cells were harvested as described above.

Fragile site FISH was performed as previously described by (Le Tallec *et al*., 2011). Probes for the common fragile sites FRA3B and FRA16D were made from BACs RP11-170K19 and RP11-281J9, respectively (Children's Hospital Oakland Research Institute) and were labelled with Biotin-conjugated nucleotides using the BIOPRIME DNA Labelling System (Invitrogen) according to manufacturer's protocol. For dioxigenin incorporation, the BIOPRIME DNA Labelling System was used, but Dioxigenin-conjugated dNTPs (Roche) were used instead of biotin-conjugated dNTPs. Probes were purified using Illustra Probequant G-50 micro columns (GE Healthcare).

Flow cytometry

Flow cytometry was carried out as described previously (Townsend *et al.*, 2009). Briefly, HeLa cells were harvested, fixed in 70% ethanol at -20°C for at least 1 h, and permeabilised with 0.25% Triton-X100 for 15 at 4°C. For immuno-detection of phospho-histone H3 (Ser10), cells were then incubated with primary antibody for 1 h, washed in 1% BSA, and counterstained with Alexa Fluor-488 goat anti-mouse IgG antibody. Cells were then washed twice with 1% BSA, and stained with 25 μg/ml propidium iodide containing 0.1 mg/ml RNase A. Cells were

analysed using an Accuri flow cytometer (BDBiosciences) in conjunction with CFlowplus software. Data represents that obtained from at least 30,000 cells.

Antibodies and Western blotting

Whole cell extracts were obtained by sonication in UTB buffer (8 M Urea, 50 mM Tris, 150 mM β-mercaptoethanol, protease inhibitor cocktail (Roche)) and analysed by SDS-PAGE following standard procedures. The following antibodies were used: H2A, γ-H2AX, BRCA2, RPA2, RAD51 (Merck Millipore); MRE11, phospho-histone H3 Ser-10, phospho-CDK2 Tyr-15 (Cell Signalling); MCM7, CHK1, PCNA, CDK2, FANCD2, BRCA1, BRCA2 (Santa Cruz Biotechnology); RECQL5, FANCA, EXO1, phospho-RPA2 Ser-4/8, phospho-CHK1 Ser-317, phospho-CHK1 Ser-345, MLL1 (Bethyl); CENPA, DNA2, BOD1, PCNT-1 (Abcam), α-tubulin, FLAG (Sigma Aldrich); GFP (Roche); BrdU (CldU) (AbD Serotec); BrdU (IdU) (Becton Dickinson); MCM2 (BD Transduction); 53BP1 (G. S. Stewart); PICH (H. Yu). Affinity purified polyclonal anti-BOD1L antibodies were generated by immunising rabbits with a purified GST-fusion protein spanning amino acids 1,900 to 2,501 of human BOD1L (Accession number: NP_683692.2) (Eurogentec).

Immunoprecipitations

HeLa nuclear cells extracts (Cilbiotech) were clarified by centrifugation at 44,000 x g, immunoprecipitated with 5 µg of anti-BOD1L antibody or IgG for 3 h at 4 °C. After further clarification, immune complexes were isolated using protein-A sepharose (GE Healthcare), and analysed by immunoblotting.

iPOND

EdU-labeled sample preparation: Logarithmically growing HeLa S3 cells (1 x 10^6 per ml) were incubated with 10 mM EdU for 10 min. Following EdU labelling, cells were fixed in 1 % formaldehyde, quenched by adding glycine to a final concentration of 0.125 M and washed in PBS three times. Collected cell pellets were frozen at -80 °C and cells were permeabilised by

resuspending in ice cold 0.25 % Triton-X/PBS at a concentration of 1-1.5 x 10^7 cells per ml and incubating on ice for 30 min. Before the Click reaction, samples were washed once in 0.5 % BSA/PBS and once in PBS.

Click reaction: Cells were incubated in Click reaction buffer for 1h at room temperature containing 10 μM azide-PEG(3+3)-S-S-biotin conjugate (Click ChemistryTools, cat. no AZ112-25), 10 mM sodium ascorbate, and 1 mM copper (II) sulfate (CuSO4) in PBS. The 'no Click' reaction contained DMSO instead of biotin-azide. Following the Click reaction, cells were washed once in 0.5 % BSA/PBS and once in PBS. Cells were resuspended in lysis buffer (50 mM Tris–HCl pH 8.0, 1 % SDS) containing protease inhibitor cocktail (Roche) and sonicated using a Diagenode Bioruptor® Plus for 40 cycles (30 sec on/30 sec off). Samples were centrifuged at 14,500 xg at 4°C for 30 min and the supernatant was diluted 1:3 with NTN buffer (100 mM NaCl, 20 mM Tris pH 7.4 and 0.05 % NP40) containing protease inhibitors. An aliquot was taken as an input sample.

Purification: Streptavidin–agarose beads (Novagen) were washed three times in NTN buffer containing protease inhibitor cocktail. 200 μl of bead slurry was used per 1x 10^8 cells. The streptavidin–agarose beads were resuspended 1:1 in NTN buffer containing protease inhibitors and added to the samples. Samples were then incubated at 4 °C for 4 h in light exclusion. Following binding, the beads were then washed 4x with 1 ml NTN buffer and protein-DNA complexes were eluted by incubating with 5mM DTT in NTN buffer. Cross-links were reversed by incubated samples in SDS sample buffer at 95 °C for 12 min. Proteins were resolved on SDS-PAGE and detected by immunoblotting, or mass-spectrometry analysis was performed on the eluates. Mass spectrometry was carried out as described previously (Adelman *et al.*, 2013). A complete mass spectrometry data set is available on request to the Corresponding Author.

Microscopy and Image Analysis

HeLa, H1299, U-2-OS, HeLa-FUCCI or A549 cells were grown on glass coverslips. DT40 cells were grown in suspension, and dropped onto poly-L-lysine coated coverslip for 15 min. Cells were washed with PBS twice before fixation. For α-tubulin, PCNT-1, PCNA, CENPA and 53BP1 immuno-detection, cells were fixed with methanol at -20 °C for 10 minutes. For PICH, FANCD2 and EdU detection, and for 53BP1 immuno-detection in FUCCI cells, cells were fixed in 3.6% paraformaldehyde for 10 min at room temperature before permeabilisation with nuclear extraction buffer (10 mM PIPES, 20 mM NaCl, 3 mM $MgCl_2$, 300 mM sucrose, 0.5% Triton X-100) for 10 minutes. For RAD51, γ-H2AX, BRCA2 and RPA immuno-detection, cells were pre-treated with nuclear extraction buffer for 5 minutes on ice, and fixed in 3.6% paraformaldehyde for 10 minutes at room temperature. For in situ detection of nascent DNA in mitotic and interphase cells the Click-iT DNA Alexa Fluor 495 Imaging Kit (Invitrogen) was used. For ssDNA (BrdU) analyses, cells were pre-treated with nuclear extraction buffer for two 5 consecutive minute incubations on ice, then fixed as above. After fixation, cells were washed with PBS three times and then blocked with ADB (Antibody Dilution Buffer; 5% FCS in PBS) for 1 h at 4°C. Cells were incubated with primary antibody (diluted in ADB) for 1 h at room temperature, washed with ADB and then counterstained with Alexa Fluor-488 goat anti-rabbit IgG, Alexa Fluor-594 goat anti-mouse IgG, Alexa Fluor-350 goat anti-rabbit IgG, or Alexa Fluor-555 donkey anti-rabbit IgG secondary antibodies (Molecular Probes) diluted in ADB, for 1 h at room temperature. Cells were then washed twice with ADB and coverslips were mounted onto glass slides with Vectashield mounting agent containing 0.4 μg/ml DAPI (Vectashield). Fluorescence images were taken using a Nikon E600 Eclipse microscope equipped with a 60X oil lens, and images were acquired and analysed using Volocity Software v4.1 (Improvision). For ssDNA analyses, BrdU foci were enhanced using the ImageJ convolve function, and the number of nuclear foci/cell quantified.

Proximity ligation assays

For proximity ligation assays (PLA), cells were fixed/permeabilised as appropriate for the primary antibodies used, incubated in primary antibody, and in situ proximity ligation was performed using Duolink Detection Kit in combination with anti-Mouse PLUS and anti-Rabbit MINUS PLA Probes, according to the manufacturer's instructions (Sigma Aldrich Duolink). Nuclear foci were imaged as above, and the number of nuclear foci/cell quantified using ImageJ.

SUPPLEMENTAL REFERENCES

Adelman, C.A., Lolo, R.L., Birkbak, N.J., Murina, O., Matsuzaki, K., Horejsi, Z., Parmar, K., Borel, V., Skehel, J.M., Stamp, G., et al. (2013). HELQ promotes RAD51 paralogue-dependent repair to avert germ cell loss and tumorigenesis. Nature 502, 381-384.

Le Tallec, B., Dutrillaux, B., Lachages, A.M., Millot, G.A., Brison, O., and Debatisse, M. (2011). Molecular profiling of common fragile sites in human fibroblasts. Nature structural & molecular biology 18, 1421-1423.

Mendez, J., and Stillman, B. (2000). Chromatin association of human origin recognition complex, cdc6, and minichromosome maintenance proteins during the cell cycle: assembly of prereplication complexes in late mitosis. Molecular and cellular biology 20, 8602-8612.

Niedzwiedz, W., Mosedale, G., Johnson, M., Ong, C.Y., Pace, P., and Patel, K.J. (2004). The Fanconi anaemia gene FANCC promotes homologous recombination and error-prone DNA repair. Molecular cell 15, 607-620.

Townsend, K., Mason, H., Blackford, A.N., Miller, E.S., Chapman, J.R., Sedgwick, G.G., Barone, G., Turnell, A.S., and Stewart, G.S. (2009). Mediator of DNA damage checkpoint 1 (MDC1) regulates mitotic progression. The Journal of biological chemistry 284, 33939-33948.

Stewart, G.S., Wang, B., Bignell, C.R., Taylor, A.M., and Elledge, S.J. (2003). MDC1 is a mediator of the mammalian DNA damage checkpoint. Nature *421*, 961-966.